HELSINKI INSTITUTE OF PHYSICS INTERNAL REPORT SERIES

HIP-2015-02

Aspects of Holographic Thermalization

Lasse Franti

Helsinki Institute of Physics
and
Department of Physics
Faculty of Science
University of Helsinki
Finland

ACADEMIC DISSERTATION

To be presented, with the permission of the Faculty of Science of the University of Helsinki, for public examination in the auditorium CK112 at Exactum, Gustav Hällströmin katu 2b, Helsinki, on the 13^{th} *of August 2015 at 12 o'clock.*

Helsinki 2015

ISBN 978-952-10-8124-8 (printed version)
ISSN 1455-0563
ISBN 978-952-10-8125-5 (pdf version)
http://ethesis.helsinki.fi
Unigrafia
Helsinki 2015

L. Franti: Aspects of Holographic Thermalization
University of Helsinki 2015, 53 pages,
HIP Internal Report Series HIP-2015-02
ISSN 1455-0563
ISBN 978-952-10-8124-8 (printed version)
ISBN 978-952-10-8125-5 (pdf version)

Keywords: gauge/gravity duality, holography, hyperscaling violation, Lifshitz scaling, quark gluon plasma, anisotropy

Abstract

The gauge/gravity duality connects the dynamics of gravity theories in the bulk with the dynamics of field theories on the boundary. In this thesis we introduce two thermalization scenarios and investigate them using a suitable holographic description.

We will first study the thermalization of equal-time correlators and entanglement entropy in a hyperscaling violating AdS-Lifshitz-Vaidya metric. This work verifies the agreement between numerical procedures and preceding analytical predictions and generalises the previous studies of thermalization in this kind of situations.

In the latter part we will use the duality to describe the quark-qluon plasma created in heavy ion collisions. The anisotropic plasma is modelled by introducing anisotropies into the source on the gravity side and letting them evolve according to the equations of motion. The boundary dynamics is extracted by finding the boundary stress-energy tensor. The results agree with the conventional models. The situations considered here are rather simple but this work demonstrates the applicability of holography in the anisotropic case.

Acknowledgements

First and foremost I want to thank my thesis supervisor Esko Keski-Vakkuri for his patience and support during my PhD-studies. I would also like to thank the pre-examiners, Tuomas Lappi and Matti Järvinen, for their contructive comments on my thesis. I am equally grateful to Niko Jokela for his remarks on the earlier versions of the draft. This thesis would not have been possible without my collaborators both in Helsinki and abroad.

I would like to thank all my roommates, especially Erik Brücken and Risto Montonen, for interesting discussions on physics and life in general. Joni Suorsa, Tuukka Meriniemi, Otso Huuska and countless other people at the Department have been part of my life during the last nine years.

The financial support from the Vilho, Yrjö and Kalle Väisälä Fund and the Finnish Academy of Science and Letters made this work possible and is gratefully acknowledged. This thesis is based on reasearch carried out at the Helsinki Institute of Physics and Department of Physics at the University of Helsinki.

Finally I would like to thank my parents and sister for putting up with me during my studies and before them.

Contents

Included papers

I: Piermarco Fonda, Lasse Franti, Ville Keränen, Esko Keski-Vakkuri, Larus Thorlacius, Erik Tonni, "Holographic thermalization with Lifshitz scaling and hyperscaling violation", JHEP 51 (2014), [arXiv:1401.6088 [hep-th]]

II: V. Balasubramanian, A. Bernamonti, J. de Boer, B. Craps, L. Franti, F. Galli, E. Keski-Vakkuri, B. Müller, A. Schäfer, "Inhomogeneous Thermalization in Strongly Coupled Field Theories", Phys. Rev. Lett. 111 (2013), [arXiv:1307.1487 [hep-th]]

III: V. Balasubramanian, A. Bernamonti, J. de Boer, B. Craps, L. Franti, F. Galli, E. Keski-Vakkuri, B. Müller, A. Schäfer, "Inhomogeneous holographic thermalization", JHEP 82 (2013), [arXiv:1307.7086 [hep-th]]

Paper I

The paper consists of two independent studies which were combined in a rather late stage. The author derived the Hyper-Lifshitz-Vaidya (HLV) metric and adapted with improvements the existing numerical procedure to investigate geodesic correlators and entanglement entropy in these spacetimes. This work is presented in section 3 and covers the path from the initial HLV metric to the final plots. After the merger, the author participated in discussions and calculations using the developed numerical scheme.

Papers II and III

The author spent a substantial time working on several prospective solution methods for the anisotropic spacetime and associated expansions. In addition to the direct solution with small boundary source with independent small perturbations, many ways to relate the expansion parameters were tried. The later successful assumption of slow spatial dependence was also included both independently and combined with the other parameters. After the solution was obtained by other collaborators, the author participated in the analytical calculations and their verification.

1 General introduction

During the last couple of years an increasing number of researchers have immersed themselves into the emerging field of gauge/gravity dualities. This paradigm has been spreading from its original kingdom of theoretically beautiful conformally invariant theories, such as the initial $N = 4$ super Yang-Mills, to new less charted but more realistic fields. These include condensed matter theory, quark gluon plasma, lattice theories and non-equilibrium dynamics. Although the initial constructions do not have a major role in the practical calculations presented here, historic consistence and even tradition compels us to include a short account on the original rigid dualities by the pioneering fathers.

1.1 Background in strings

Originally developed to explain the Regge trajectories of meson and baryon resonances, string theory has become one of the most prominent topics in mathematical physics. One of the issues faced in this hadron model era was the existence of massless spin-2 particles in these theories. As QCD proved to be a much more natural and accurate theory of quarks and gluons, string theory became somewhat less interesting in this context. The tensor particle, however, made string theory a possible candidate for quantum gravity. The particle content also gives a distant hope of even unifying all existing theories into a single theory of everything. However, string theory is still hampered by many existing issues, such as its overwhelming sortiment of different possible vacua and the very high energy scales of observable predictions.

One of the most active branches of contemporary theoretical physics, the gauge/gravity duality, was born in 1997 when Juan Maldacena [1] proposed that in at least one particular case string and field theories are connected in a much more surprising way. Moreover this connection is very strong. This discovery was preceded by the holographic principle proposed by 't Hooft and elucidated by Susskind [2], but the discovery by Maldacena and the subsequent work by Gubser, Klebanov, Polyakov [3] and Witten [4] made the connection between gauge and string theories much more concrete. After this initial discovery, a multitude of more or less specific holographic models have emerged, making Maldacena's paper one of the most cited articles in the history of physics.

1.2 The AdS/CFT duality

The exact form of the Maldacena duality states that $N = 4$ $U(N)$ super-Yang-Mills theory in 3+1 dimensions is dual to type IIB superstring theory on $AdS_5 \times S_5$. The correspondence is thought to be exact, although no mathematically rigorous proof exists. Unfortunately, the concrete use of this duality is impeded by the rather complicated construction of the theories involved. On the AdS-side there is a string theory living on the product of a five-dimensional space with hyperbolic behaviour and a hypersphere, and the field theory side is a supersymmetric $N = 4$ Yang-Mills theory ($N = 4$ SYM),

which is conformal and has a fairly complicated Lagrangian. The gauge and string sides are thus both highly nontrivial. $N = 4$ SYM is also not very close to any observable theory of nature and, in particular, its behaviour is qualitatively different from QCD, which is confining and non-conformal.

The practical use of the AdS/CFT-correspondence thus requires one to consider various limits. Many toy models do not really aspire to describe nature but are studied to investigate the dynamics of the duality itself. These so-called non-physical models seem to be especially frequently utilized in AdS/QCD. These models usually show phenomena reminiscent of real QCD dynamics, but are not very satisfactory due to nonphysical assumptions, such as a wrong number of colours or extreme limits. Many models assume N to be very large, which enables the use of supergravity in the bulk and $1/N$ -expansions in the field theory side. Large-N limits are widely used in holographic QCD, although in physical situations $N = 3$.

Even though strings are no longer prominent in most practical gauge/gravity models, the original duality is still relevant as a somewhat rigorous holography scheme. Several groups are trying to derive practical models top-down from the multi-dimensional branes to the level of field theories and thermalization problems.

Some features of the original duality are still present in most holographic models. One of these is the use of anti-de Sitter space and its flat boundary to house the bulk and boundary dynamics.

1.3 The AdS-geometry

The pure anti-de Sitter space describes the geometry of an empty spacetime with a negative cosmological constant. This spacetime can be written down using several different coordinates, each describing different patches of the full space. One can define the AdS_n space as a hyperboloid of the form

$$x_1^2 + \ldots + x_{n-1}^2 - Y^2 - Z^2 = -1 \tag{1}$$

in a flat space with the metric

$$ds^2 = dx^2 + \ldots + dx_{n-1}^2 - dY^2 - dZ^2. \tag{2}$$

If we set $n = 2$ this can be interpreted as a hyperboloid embedded in a three dimensional Minkowski space.

A somewhat more illuminating and definitely more usable form is the induced metric on the hyperboloid in Poincaré coordinates

$$ds^2 = \frac{1}{y^2}(-dt^2 + dy^2 + dx^2 + \ldots + dx_{n-2}^2). \tag{3}$$

This can be easily interpreted as a conformally flat space equipped with one special spatial coordinate. In applications it is common to use the inverse coordinate $r = 1/y$

and the resulting metric

$$ds^2 = -r^2 dt^2 + \frac{dr^2}{r^2} + r^2(dx^2 + \ldots + dx_{n-2}^2). \tag{4}$$

The scaling of the transverse directions suggests that the inverse coordinate can be interpreted as a radius. With the light-cone ansatz

$$v = t + \frac{1}{r} \tag{5}$$

one obtains the Eddington-Finkelstein form

$$ds^2 = -r^2 dv^2 + 2drdv + r^2 dx_i^2. \tag{6}$$

These forms are used throughout this introduction. One can also express the metric in spherical coordinates to obtain

$$ds^2 = -(1+\rho^2)dt^2 + \frac{d\rho^2}{1+\rho^2} + \rho^2 d\Omega_{n-2}\,. \tag{7}$$

From (3), (4), and (7) one can see that the boundary $y = 0$, $r \to \infty$ is conformally flat. In Poincaré coordinates this is manifestly visible from the metric. This is very important, as the field theory lives on the AdS boundary.

2 Hydrodynamics from gravity

Having examined the canonical cases, we can now concentrate on the actual topic of this thesis. This requires us to drop some of the mathematical rigor in exchange of more realistic situations on the field theory side. This kind of trade-off is not uncommon in bottom-up models such as the ones included in this thesis. Before presenting the models used in the accompanying papers, let us examine a purely analytic procedure to derive classical hydrodynamics from a gravity solution to illustrate the philosophy of introducing dynamics and reading off results for the dual theory. This review is based on two papers [5] and [6], which complement each other in a rather nice way.

2.1 Scaling symmetry and hydrodynamic limit

It can be seen that the nonrelativistic Navier-Stokes equations for incompressible fluid

$$\partial^i v_i = 0 \tag{8}$$

$$\partial_t v_i - \eta \partial^2 v_i + \partial_i P + v^j \partial_j v_i = 0 \tag{9}$$

retain their form in the rescaling of velocity and pressure

$$\begin{aligned} v_i^\epsilon(x^i, \tau) &= \epsilon v_i(\epsilon x^i, \epsilon^2 \tau) \\ P^\epsilon(x^i, \tau) &= \epsilon^2 P(\epsilon x^i, \epsilon^2 \tau)\,. \end{aligned} \tag{10}$$

This means that rescaled quantities obey the same equations, i.e.,

$$\partial^i v_i^\epsilon = 0 \tag{11}$$

$$\partial_t v_i^\epsilon - \eta \partial^2 v_i^\epsilon + \partial_i P^\epsilon + v^j \partial_j v_i^\epsilon = 0\,. \tag{12}$$

The most important feature, however, is the scaling of allowed corrections to (9) under this transformation. From general considerations we know that these extra terms should vanish in the hydrodynamic description of incompressible Newtonian fluids. We can indeed achieve this by using the scaling symmetry and studying the resulting equations in the limit of very small ϵ. This scaling is thus called the hydrodynamic scaling, as all reasonable corrections to the classic Navier-Stokes equations vanish at the limit $\epsilon \to 0$. The hydrodynamic limit can thus be rather explicitly represented in this way.

2.2 The stress tensor

Extracting the field theory dynamics from a gravity solution can be made in different ways. We will calculate the Brown-York stress tensor, which we will show to be similar to the stress-energy of an incompressible fluid. This correspondence is demonstrated by deriving the equations of motion for an incompressible fluid from the energy-momentum tensor.

The Brown-York stress-energy was derived in [7] where it was presented as a quasi-local energy momentum tensor associated with hard spacetime boundaries which in practice are usually realized as cutoff surfaces. According to this proposition, the energy-momentum tensor can be calculated from the expression

$$T_{ab} = 2(\gamma_{ab}K - K_{ab}) \tag{13}$$

where K_{ab} is the extrinsic curvature of the boundary and K is its trace taken with respect to the boundary metric γ_{ab}.

The extrinsic curvature can be calculated as

$$K_{ab} = \frac{1}{2}\left(\mathcal{L}_{\mathcal{N}} g_{\alpha\beta}\right) e_a^\alpha e_b^\beta = \left(\nabla_\alpha N_\beta\right) e_a^\alpha e_b^\beta \tag{14}$$

where we use covariant derivatives with respect to the full metric. Here Greek indices refer to the bulk spacetime and latin indices to the boundary. The transformation matrices

$$e_a^\alpha = \left(\frac{\partial x^\alpha}{\partial x^a}\right) \tag{15}$$

are constant for coordinate surfaces, which makes our calculation considerably simpler.

2.3 Boosted black hole

The worldview of an accelerating observer in Minkowski space is described by the Rindler metric

$$ds^2 = -r d\tau^2 + 2dr d\tau + dx^2 \,. \tag{16}$$

This metric can be made dynamic by performing boosts of the form

$$\sqrt{r_c}\tau \to \gamma\sqrt{r_c}\tau - \gamma\beta_i x^i \tag{17}$$

$$x^i \to x^i - \gamma\beta^i\sqrt{r_c}\tau + (\gamma - 1)\frac{\beta^i\beta_j}{\beta^2}x^j \tag{18}$$

with

$$\gamma = (1-\beta^2)^{-1/2} \qquad \beta_i = r_c^{-1/2} v_i \,, \tag{19}$$

which introduces an arbitrary velocity v_i. Another parameter can be added by a shift in the radial coordinate

$$r \to r - r_h \tag{20}$$

followed by the rescaling

$$\tau \to (1 - r_h/r_c)^{-1/2}\tau \,. \tag{21}$$

Applying these transformations in the above order leads to the expression

$$\begin{aligned} ds^2 = {} & \frac{d\tau^2}{1 - v^2/r_c}\left(v^2 - \frac{r - r_h}{1 - r_h/r_c}\right) + \frac{2\gamma}{\sqrt{1 - r_h/r_c}} d\tau dr - \frac{2\gamma v_i}{r_c\sqrt{1 - r_h/r_c}} dx^i dr \\ & + \frac{2v_i}{1 - v^2/r_c}\left(\frac{r - r_c}{r_c - r_h}\right) dx^i d\tau + \left(\delta_{ij} - \frac{v_i v_j}{r_c^2(1 - v^2/r_c)}\left(\frac{r - r_c}{1 - r_h/r_c}\right)\right) dx^i dx^j \,. \end{aligned} \tag{22}$$

We will define the pressure in terms of the radial shift r_h as

$$p = \frac{1}{\sqrt{r_c - r_h}} \tag{23}$$

and consider the actual hydrodynamic quantities to be small perturbations with coordinate dependence, which allows us to write

$$v_i = v_i^{(\epsilon)}(\tau, x_j) \qquad p = r_c^{-1/2} + r_c^{-3/2} P^{(\epsilon)}(\tau, x_j)\,. \tag{24}$$

Using the hydrodynamic scaling

$$v_i^{(\epsilon)}(\tau, x_j) = \epsilon v_i(\epsilon^2\tau, \epsilon x_j), \qquad P^{(\epsilon)}(\tau, x_j) = \epsilon^2 P(\epsilon^2\tau, \epsilon x_j) \tag{25}$$

we obtain the approximate result

$$\begin{aligned} ds^2 = -r d\tau^2 + 2d\tau dr + dx_i dx^i - 2\left(1 - \frac{r}{r_c}\right) v_i dx^i d\tau - \frac{2v_i}{r_c} dx^i dr \\ + \left(1 - \frac{r}{r_c}\right)\left[(v^2 + 2P)d\tau^2 + \frac{v_i v_j}{r_c} dx^i dx^j\right] + \left(\frac{v^2}{r_c} + \frac{2P}{r_c}\right) d\tau dr + O(\epsilon^3)\,. \end{aligned} \tag{26}$$

Let us now introduce the cut-off surface at $r = r_c$. The normal vector with respect to the full metric is

$$N^\mu \partial_\mu = \frac{1}{\sqrt{r_c}}\partial_\tau + \sqrt{r_c}\left(1 - \frac{P}{r_c}\right)\partial_r + \frac{v^i}{\sqrt{r_c}}\partial_i + O(\epsilon^3)\,. \tag{27}$$

Using equations (13) and (14) we can calculate the Brown-York stress tensor for the cutoff surface and determine the associated equations of motion in the boundary theory using covariant conservation laws.

The first nontrivial equation appears at order ϵ^2 and reads

$$r_c^{3/2} \partial_a T^{a\tau} = \partial_i v^i = 0\,. \tag{28}$$

This is simply the condition for an incompressible fluid. Using this condition, we can express the energy-momentum tensor in the form given in [6]

$$T_{ij} dx^i dx^j = \frac{dx_i^2}{\sqrt{r_c}} + \frac{v^2}{\sqrt{r_c}} d\tau^2 - 2\frac{v_i}{\sqrt{r_c}} dx^i d\tau + \frac{v_i v_j + P\delta_{ij}}{r_c^{3/2}} dx^i dx^j - 2\frac{\partial_i v_j}{\sqrt{r_c}} dx^i dx^j + O(\epsilon^3)\,. \tag{29}$$

The rest of the time component $\partial_a T^{a\tau}$ is of fourth order or higher, so we can move to the spatial components $\partial^a T_{ai}$, which are of third order. By interpreting the bulk speed of light $\sqrt{r_c}$ as the square root of viscosity, one obtains

$$r_c^{3/2} \partial^a T_{ai} = \partial_\tau v_i - \eta \partial^2 v_i + \partial_i P + v^j \partial_j v_i = 0 \tag{30}$$

i.e. the Navier-Stokes equation.

It is good to note that the field theory lives in the flat boundary. The Navier-Stokes equation we obtained is thus describing a fluid in flat space, as is classically the case.

The main motivation for presenting this calculation is its philosophical structure, which is very typical of holographic calculations. A suitable static metric is first chosen to fit the needs of the calculation. Time dependent behaviour is introduced by perturbing the metric in some way and the dynamics extracted by examining relevant boundary quantities and re-interpreting the bulk variables in terms of the boundary theory. The following two sections follow this philosophy to investigate thermalization in two different boundary theories.

3 Hyperscaling violation and Lifshitz scaling

The total number of holographic models introduced is immense and even established fields within holography are numerous. Condensed matter applications include holographic superfluids [8], and electron stars [9], [10] as models of Fermi surfaces. The term electron star or cloud refers to the bulk configuration with an ideal fluid of fermions supported by a chemical potential in a gravitational field. The pursued dual theory is similarly a system of strongly interacting fermions. AC and DC conductivities for different models have been calculated, see [11]. For short review papers on the various condensed matter applications, see [12] and [13]. Studying the entanglement entropy in non-relativistic field theories is also a major motivation for Lifshitz holography, see [14] and [15]. Violations of the area law for Fermi surfaces [16] have been studied using hyperscaling violation, see [17], [18] and references therein.

The Vaidya metric itself was first introduced by Prahalad Vaidya in 1951 [19] and refined in [20]. This metric describes a spherically symmetric spacetime with either inflowing or outflowing null dust, for which he most natural example is a nonrotating star. We will use the asymptotically anti-de Sitter version, which is more suitable for holography and has by now been used in numerous papers including [21] ,[22], and [23]. The precursor for this work was [24], which investigated holographic thermalisation and entanglement by using the time dependent Lifshitz-Vaidya metric with collapsing null dust. Its approach was a descendant of [25], which introduced the Einstein-Dilaton-Maxwell theory in this setting. This field content is sufficient to give rise to spacetimes with time dependence and Lifshitz scaling. In another paper [27] Alishahiha et al discussed entanglement in the case of Lifshitz geometries with added hyperscaling violation. This paper used the same ingredients to realize the required spacetimes and cited [25] as its main reference. In the paper [I] we investigated these matters in the time dependent Hyper-Lifshitz-Vaidya metric with both hyperscaling violation and a nonrelativistic dynamical exponent.

The leading idea in these calculations is to model thermalization by a gravitational process. The initial vacuum corresponds to a field theoretic vacuum. By changing the metric, we get a non-equilibrium state which evolves into a thermal state represented by a black hole on the gravity side. The prominent role of the Vaidya metric is based on the lightlike collapse as the falling shell remains static in Eddington-Finkelstein time.

In paper [I] we developed a holographic model for thermalization following a quench near a quantum critical point with non-trivial dynamical critical exponent and hyperscaling violation. In this work the anti- de Sitter Vaidya null collapse geometry was generalized to a Hyper-Lifshitz-Vaidya metric. Non-local observables such as two-point functions and entanglement entropy in this background then provide information about the length and time scales relevant to thermalization. The project started as a collaboration of the author with Esko Keski-Vakkuri and Ville Keränen. The project had advanced to a late stage when we came aware of the other group led by Erik Tonni. The resulting paper [I] thus consists of two rather independent calculations with two

separate codes. The discussion here follows the route taken by the author and mainly considers the results of this work.

3.1 Hyper-Lifshitz-Vaidya solutions

A bottom-up Einstein-Maxwell-Dilaton (EMD) gravity model with static hyperscaling violating Lifschitz-AdS black brane solutions was introduced in [27]. In this section we briefly review the model with its black brane solutions and generalize these results by deriving a time-dependent solution describing a null collapse of a (flat) shell to a black brane, which gives rise to the hyperscaling violating Lifschitz-AdS Vaidya metric (Hyper-Lifshitz-Vaidya).

Following [27] we work with the model

$$S = -\frac{1}{16\pi G}\int d^{d+2}\sqrt{-g}\left[R - \frac{1}{2}(\partial\phi)^2 + V_0 e^{\gamma\phi} - \frac{1}{4}\sum_{i=1}^{2} e^{\lambda_i\phi}F_i^2\right]. \tag{31}$$

The bulk spacetime dimension is $D+1 = d+2$ so the spacetime boundary of the asymptotically AdS solutions will be $D = d+1$ dimensional. In addition to gravity, the EMD action contains two gauge fields and a scalar. The potential term and the coupling constants of the gauge fields also depend on the scalar field. The strength of the potential and coupling is controlled by four parameters $\gamma, \lambda_1, \lambda_2$ and V_0.

The equations of motion obtained directly from this action read

$$R_{\mu\nu} - \frac{1}{2}Rg_{\mu\nu} = \frac{1}{2}\left[\partial_\mu\phi\partial_\nu\phi + g_{\mu\nu}\left(-\frac{1}{2}\partial_\mu\phi\partial^\mu\phi + V_0 e^{\gamma\phi}\right)\right] \tag{32}$$
$$+\frac{1}{2}\sum_{i=1}^{N} e^{\lambda_i\phi}\left(F^i_{\mu\alpha}F^{i\,\alpha}_{\nu} - \frac{1}{4}g_{\mu\nu}F^i_{\alpha\beta}F^{i\,\alpha\beta}\right)$$

$$\frac{1}{\sqrt{-g}}\partial^\mu\sqrt{-g}\partial_\mu\phi + V_0\gamma e^{\gamma\phi} - \frac{1}{4}\sum_{i=1}^{N}\lambda_i e^{\lambda_i\phi}F^i_{\mu\nu}F^{i\,\mu\nu} = 0 \tag{33}$$

$$\nabla_\mu\left(e^{\lambda_i\phi}F^{i\,\mu\nu}\right) = 0\,. \tag{34}$$

As shown in [27], this theory has static hyperscaling violating Lifshitz black brane solutions with charge. The required dynamical and hyperscaling violating exponents

(ζ, θ) define the metric and the source fields as

$$\begin{aligned} ds^2 =& r^{-2\theta/d}\left(-r^{2\zeta}f(r)dt^2 + \frac{dr^2}{r^2 f(r)} + r^2 d\vec{x}^2\right) \\ F_{1rt} =& \sqrt{2(\zeta-1)(\zeta+d-\theta)}\exp\left(-\frac{d+\theta(1-d)/d}{\sqrt{2(d-\theta)(\zeta-1-\theta/d)}}\phi_0\right) r^{d+\zeta-\theta-1} \\ F_{2rt} =& Q\sqrt{2(d-\theta)(\zeta-\theta+d-2)}\exp\left(-\sqrt{\frac{\zeta-1-\theta/d}{2(d-\theta)}}\phi_0\right) r^{-(d+\zeta-\theta-1)} \\ e^{\phi} =& e^{\phi_0} r^{\sqrt{2(d-\theta)(\zeta-1-\theta/d)}} \end{aligned} \tag{35}$$

with the blackening factor

$$f(r) = 1 - \frac{m}{r^{\zeta+d-\theta}} + \frac{Q^2}{r^{2(\zeta+d-\theta-1)}}\,. \tag{36}$$

The free parameters m, Q are the mass and the charge of the brane. The intial value of the scalar field ϕ_0 is not important and could be set to zero, which simplifies the equations.

The dynamical and hyperscaling violating exponents are also related to the parameters appearing in the action. For the relations it is convenient to introduce $\alpha = -\theta/d$ and $\beta = \sqrt{2d(1+\alpha)(-1+\zeta+\alpha)}$. With these definitions we can express the parameters as

$$V_0 = (\alpha d + \zeta + d - 1)(d\alpha + \zeta + d)\exp\left(\frac{2\alpha\phi_0}{\beta}\right) \tag{37}$$

$$\gamma = -2\alpha/\beta \tag{38}$$

$$\lambda_1 = -2(\alpha(d-1)+d)/\beta \tag{39}$$

$$\lambda_2 = \sqrt{\frac{2(\alpha+\zeta-1)}{d(\alpha+1)}}\,. \tag{40}$$

Based on this static solution and work done in [24], we can hope to find a hyperscaling-violating Lifshitz-Vaidya (HLV) metric with nonzero hyperscaling exponent. Following [24], we shall make an ansatz for the HLV metric by adding time dependencies to the functions. We will then show that this metric is a solution of the Einstein-Dilaton-Maxwell equations with an additional term in the energy-momentum tensor.

As demonstrated, the static hyper-Lifshitz metric

$$ds^2 = r^{-2\frac{\theta}{d}}(-r^{2\zeta}f(r)dt^2 + \frac{dr^2}{r^2 f(r)} + r^2 dx^2) \tag{41}$$

with

$$f(r) = 1 - \frac{m}{r^{\zeta+d-\theta}} \tag{42}$$

can be realized for arbitrary values of the parameters ζ and θ. We can transform this into a Eddington-Finkelstein form by performing a specific transformation given by

$$dv = dt + \frac{r^{-\zeta-1}}{f(r)}dr\,, \tag{43}$$

which yields the form

$$ds^2 = r^{-2\frac{\theta}{d}}(-r^{2\zeta}f(r)dv^2 + 2dvdrr^{\zeta-1} + r^2dx^2)\,. \tag{44}$$

As promised earlier, we shall try to generalize the static solution by simply making the blackening factor (42) time-dependent. More boldly, we can try to achieve this by just making the mass time-dependent and observing the corresponding changes in the energy-momentum tensor. We shall therefore assume a metric Ansatz of the form

$$ds^2 = r^{-2\frac{\theta}{d}}(-(1 - \frac{m(v)}{r^{\zeta+d-\theta}})r^{2\zeta}dv^2 + 2dvdrr^{\zeta-1} + r^2dx^2) \tag{45}$$

and analyze the resulting equations of motion. With some precognition from [24], we can try to search for a source consisting of the same source fields and a modified time-dependent matter component. From now on we will set $d = 2$ and use $\mu = \exp(\phi_0)$.

Following [24] and [27] we can use a radial gauge. This allows us to write

$$\phi = \mathrm{Log}(\mu r^{\sqrt{2(2-\theta)(\zeta-1-\theta/2)}}) \tag{46}$$

and

$$A_v = \sqrt{\frac{2(z-1)}{2+\zeta-\theta}}\mu^{-\frac{\theta-4}{2\sqrt{(2-\theta)(2-2\zeta+\theta)}}}r^{2+\zeta-\theta}, \tag{47}$$

which results in a field strength given by

$$F_{rv} = \sqrt{2(\zeta-1)(2+\zeta-\theta)}\mu^{\frac{2-\theta/2}{\sqrt{2(2-\theta)(\zeta-1-\theta/2)}}}r^{1+\zeta-\theta}\,. \tag{48}$$

The equations of motion remain in the same form as in the case without time dependence. By feeding the equations of motion with the modified metric, we can confirm that the time-dependent mass can be introduced by simply adding the extra term

$$E_{vv} = \frac{1}{2}(2-\theta)\frac{m'(v)}{r^{2-\theta}} \tag{49}$$

to the bulk energy-momentum tensor appearing on the right hand side of (32). This term is analogous to the case without hyperscaling violation and reduces to the result found in [24] if we set $\theta = 0$. The modified exponent in the denominator seems quite natural taking into account the scaling of area in the metric and the interpretation as infalling massless matter. Although this demonstration is not absolutely necessary for our discussion, the possibility to source the HLV metric with a somewhat standard field content is naturally a very positive feature.

3.2 The Hyper-Lifshitz-Vaidya metric

The main features of the HLV metric are the two exponents ζ and θ which govern the deviation from hyperscaling and the relativistic relation between space and time. In the absence of hyperscaling ($\theta = 0$), the vacuum metric

$$ds^2 = r^{-2\theta/d}\left(-r^{2\zeta}dt^2 + \frac{dr^2}{r^2} + r^2 d\vec{x}^2\right) \tag{50}$$

remains invariant in the scaling

$$t \to \lambda^\zeta t \quad x \to \lambda x \quad r \to \lambda^{-1} r\,. \tag{51}$$

This kind of behaviour is called Lifshitz scaling and it is observed in models of quantum systems and even phase diagrams of known materials [28] which is one of the motivations to study this kind of theories. The standard relativistic scaling is restored if we set $\zeta = 1$.

If the hyperscaling exponent θ is nonzero, the metric (50) retains its form under (51) with an overall scaling

$$ds \to \lambda^{\theta/d} ds\,. \tag{52}$$

This corresponds to hyperscaling violation in the dual theory: Instead of the usual scaling relation of entropy and temperature

$$S \propto T^{d/\zeta} \tag{53}$$

we have [26] [27]

$$S \propto T^{(d-\theta)/\zeta}\,. \tag{54}$$

Roughly speaking the hyperscaling exponent lowers the apparent thermodynamical dimension by θ from d to $d_\theta = d - \theta$.

The third parameter after ζ and θ is the mass of the brane, which can be set to an arbitrary value without introducing extra sources to the metric. As shown in the previous chapter, a "time-dependent" solution with $m(v)$ can be realized by introducing an extra term to the energy momentum tensor. The dependence on the Eddington-Finkelstein time and radial coordinate indicates that this term corresponds to a shell of pressureless lightlike dust with the natural scaling of density.

The fourth parameter is the charge which we have chosen to be zero. This choice has also been done in [24] and [29] where similar investigations were carried out in Lifshitz-Vaidya and HLV. The main interest in geodesic correlators and entanglement entropy is focused on the two violation exponents. The blackening factor as a whole is used as a quench parameter with a simple turn-on and convenient dynamics in Eddington-Finkelstein coordinates. Even though static and even time-dependent charges are possible, they are not relevant in studying thermalization in these models.

3.3 Geodesic correlators and entanglement entropy

To probe the thermalization of the field theory dual of the collapsing shell spacetime, we consider two sets of non-local observables, two point correlators in the geodesic approximation and the holographic entanglement entropy. In this section we review the basic definitions of these quantities.

Bulk two point functions can be computed using world line path integrals[30]

$$G(x_2, x_1) = \int_{x(t_1)=x_1}^{x(t_2)=x_2} \mathcal{D}x e^{iS[x]} \tag{55}$$

where x_1 and x_2 are the end points of the world line and $S[x]$ is the particle action.

The particle action is proportional to the mass m of the particle. Thus, in the limit of large m the path integral can be approximated by the saddle point value

$$G(x_1, x_2) \approx e^{iS_{cl}} \,. \tag{56}$$

This approximation corresponds to replacing all possible paths in space by the most probable path i.e. the classical trajectory. At the limit we get purely classical behaviour, which is a geodesic. The action of the particle is given by

$$S_{cl} = -m \int d\lambda \sqrt{-g_{\mu\nu} \frac{dx^\mu}{d\lambda} \frac{dx^\nu}{d\lambda}} \,. \tag{57}$$

In the following we are interested in equal time correlators for which it is more convenient to use a modified action

$$S = m \int d\lambda \sqrt{g_{\mu\nu} \frac{dx^\mu}{d\lambda} \frac{dx^\nu}{d\lambda}} \,, \tag{58}$$

which takes real values for spacelike geodesics. In terms of this action the correlator reads

$$G(x_2, x_1) \approx e^{-S} \tag{59}$$

and the boundary theory correlation function is obtained as a limit of this as the points x_1 and x_2 approach the boundary. In the following we consider geodesics ending on an equal time slice in the boundary [31]. Thus, we parametrize each of them using the Eddigton-Finkelstein coordinates $1/r = z = z(x), v = v(x)$ and require that z' and v' both vanish at the turning point of the geodesic, chosen to be located at $x = 0$.

We are especially interested in the thermalization time of equal time correlators in HLV metrics. The thermalization time is found by finding the values of time and boundary separation at the intersection of thermal and time dependent solutions. Along the intersection curve time dependent and thermal geodesics with same endpoints have the same length, which signifies the transition to a thermal state.

The other observable of interest is holographic entanglement entropy. In the case of static geometries the entanglement entropy is given by the famous area law

$$S_{ent} = \frac{A_{min}}{4G_N}, \tag{60}$$

where A_{min} is the $(1, d-1)$-dimensional minimum area surface ending on the boundary of the entangling region on the spacetime boundary at $z = 0$. This connection between the minimal surface and entropy was first proposed by Ryu and Takayanagi in their renowned paper [32] and worked further in [33]. The proposal is nowadays well established and widely used in holographic calculations, although the microscopic picture is not well known.

The minimum area surface is unique and well defined in the case of Euclidean spacetimes. In the case of static geometries, the Euclidean result can be safely continued to Lorentzian spacetimes, where the surface is no longer a minimal area surface but it is a saddle point of the area functional

$$A = \int d^2\sigma \sqrt{\det P(g)}, \tag{61}$$

where $P(g)$ is the induced metric on that surface. Here we will specialize to the case where the bulk spacetime is (3+1)-dimensional.

For the Vaidya case the entanglement entropy formula has to be generalized to non-static Lorentzian spacetimes. The proposal is simply to replace the area of the minimal surface by a suitable saddle point of the area functional (61), which in general is not the minimum area surface [34].

Currently no derivation of this formula exists (except for some special cases) for non-static spacetimes. Still at least within the class of Vaidya geometries, the entanglement entropy proposal satisfies many of the desired features of the entanglement entropy of a sensible quantum system (see e.g. [35]). We shall thus assume that the entanglement entropy formula (60) indeed gives the boundary theory entanglement entropy.

In the following we will consider the entanglement entropy of a rectangular boundary region $x \in (-\ell/2, \ell/2)$ and $y \in (-L/2, L/2)$ with $L \gg \ell$. With this separation of scales we can well approximate the minimal surface by a surface translationally invariant in the y direction. Thus, we can parametrize the minimal surfaces in the bulk by two functions $z = z(x)$ and $v = v(x)$. As in the geodesic case, z' and v' have to vanish at the turning point of the surface, which is located at $x = 0$.

3.4 Geodesic results

We can calculate the geodesic length and boundary time as a function of the boundary distance between the correlated points. As discussed in the previous chapter the values of boundary separation and time are connected to equal-time correlators of some operator

O in the boundary theory, since heavy fields correspond to particles travelling along geodesics. We thus write

$$\langle O(x)O(y)\rangle \propto \exp \int d\tau \sqrt{g_{\mu\nu}\frac{dx^\mu}{d\tau}\frac{dx^\nu}{d\tau}}\,. \tag{62}$$

For this calculation, we shall use the inverse radial coordinate $z = 1/r$ and the corresponding metrics. In the Schwarzschild -like coordinates of (41) the transformation is very straightforward and we get the form

$$ds^2 = z^\theta\Big(- z^{-2\zeta}b(z)dt^2 + \frac{dz^2}{z^2 b(z)} + \frac{d\mathbf{x}^2}{z^2}\Big)\,. \tag{63}$$

Transforming the Eddington-Finkelstein form (45) yields

$$ds^2 = z^\theta\left(-z^{-2\zeta}b(z,v)dv^2 - 2dvdzz^{-\zeta-1} + z^{-2}d\mathbf{x}^2\right) \tag{64}$$

with

$$b(z,v) = 1 - m(v)z^{\zeta+d-\theta}. \tag{65}$$

The equations of motion can be found from the action with the transformed metric (64). By symmetry, we can take the geodesic to have $y = const.$ We can also use x to parametrize the geodesic in a simple way, i.e.

$$z = z(x), v = v(x)\,. \tag{66}$$

Taking these choices and following the geodesic approximation, the Lagrangian is given by

$$L = \sqrt{z^{\theta-2} - 2z'v'z^{-1+\theta-\zeta} - v'^2 z^{\theta-2\zeta}b(z,v)}\,. \tag{67}$$

The two Lagrange equations can be combined to obtain

$$zv'' + \left(1-\frac{\theta}{2}\right)\left(2z'v' - z^{1-\zeta}\right) + \left(\zeta - \frac{\theta}{2}\right)z^{1-\zeta}b(z,v)v'^2 - \frac{1}{2}z^{2-\zeta}\partial_z b(z,v)v'' = 0\,. \tag{68}$$

The other equation is qiven by the "conserved" Hamiltonian and its value calculated at the turning point $z(0) = z_*$ and reads

$$1 - 2z^{1-\zeta}z'v' - z^{2-2\zeta}b(z,v)v'^2 = \frac{z_*^{2-\theta}}{z^{2-\theta}}\,. \tag{69}$$

The necessary initial conditions are given at the turning point which we fix to be located at $x = 0$. The turning point values

$$z(0) = z_* \quad \text{and} \quad v(0) = v_* \tag{70}$$

turn out to have a major influence on the geodesic behaviour and thus act as governing parameters of our calculation. We shall consider symmetric geodesics with

$$z'(0) = 0 = v'(0) \tag{71}$$

to have equal time correlators and solve the geodesic equations of motion for different turning point values z_* and v_* numerically.

For concrete numerical solutions the explicit form of the time-dependent mass function $m(v)$ has to be defined. We shall turn on the mass smoothly by using the hyperbolic tangent function and write

$$m(v) = \frac{1}{2}(1 + \tanh(v/v_0)) \tag{72}$$

which according to our interpretation of equation (49) simulates a falling shell of finite thickness. The value of v_0 is chosen to be small to have a smooth but rapid mass quench.

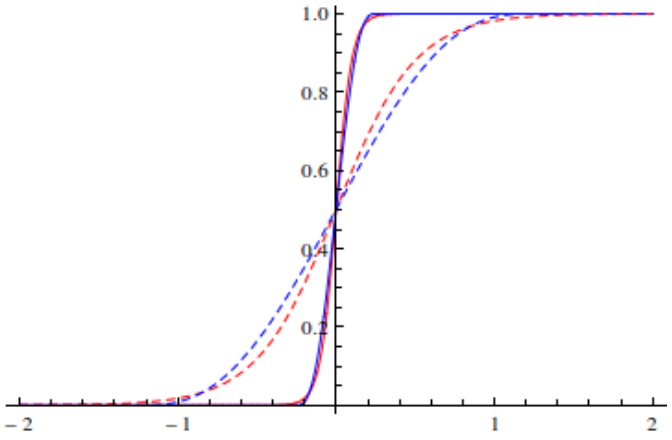

Figure 1: Comparison of the smooth turn-on functions (72) (red) and (73) (blue) with ten and fifty times the value of v_0 used in the main calculation. The actual value results in a nearly perfect step function with respect to the timescale of the dynamics.

The thermalization process is examined by generating data triplets consisting of the boundary time and separation together with the geodesic length. Geodesics probing the inner AdS-geometry are time dependent whereas the ones completely outside the forming horizon are thermal. Thermalization occurs when the thermal geodesic becomes shorter than the time-dependent alternative with the same endpoints.

In the numerical procedure the values of z at the turning point are set to suitable values inside the horizon for each of the hyperscaling exponents and the turning point time changed in diminishing steps while the corresponding boundary time and distance are recorded along with the geodesic length. The results are normalized by subtracting

the vacuum length of the geodesic from the result, which sets the value to zero before the mass quench and makes the results easier to interpret. The vacuum calculation can be done analytically, as demonstrated in the following section. The renormalized length plotted in the figures is thus the logarithm of the rescaled equal-time correlator G/G_0. The integrals are divergent and must be regulated by stopping slightly before reaching the boundary. The same distance is used for all values and situations.

The time independent thermal data is generated similarly by approaching the horizon from outside and keeping the turning point time fixed. The data triplets are then recorded and plotted in the same way, resulting in a figure like 2. The intersection curve is extracted by separately fitting a surface to the two data sets, as illustrated by figure 3. The intersection of these two surfaces represents the transition from a time dependent initial state to a time independent thermal state. The intersection curve thus represents the thermalization time as a function of boundary separation, as discussed earlier.

Using this scheme, we examined the thermalization of equal-time correlators as a function of boundary separation with various values of the hyperscaling exponent θ and obtained the results given in figure 4. We also verified that the exact functional form of the mass function is not important as the results remain essentially unchanged if (72) is replaced with some other step-like function, such as the piecewise polynomial

$$f(t) = \begin{cases} 0 & t < 0 \\ 6t^5 - 15t^4 + 10t^3 & 0 < t < 1 \\ 1 & t > 1 \end{cases} \tag{73}$$

with

$$t = \left(\frac{v}{5v_0} + 0.5 \right) \tag{74}$$

The exact speed of the quench is not important, either. Artefacts from the turn-on function start to appear only if the time dependence is strikingly slow, which corresponds to a thick shell. The two turn-on functions are illustrated in figure 1.

3.5 Geodesic vacuum

For the purpose of normalizing the results we need to know the geodesic lengths in the hyperscaling vacuum spacetime given by the metric

$$ds^2 = z^\theta (-z^{-2\zeta} dt^2 + \frac{dz^2}{z^2} + \frac{dx^2}{z^2}) \,. \tag{75}$$

The Lagrangian has no explicit x-dependence, which allows us to construct the conserved Hamiltonian

$$H = \frac{\partial L}{\partial z'} z' - L = -\frac{z^{\frac{\theta}{2}-1}}{\sqrt{1 + (z')^2}} \tag{76}$$

This means that we can express the on-shell Lagrangian as

$$L = z^{\theta-2} z_*^{1-\frac{\theta}{2}} \tag{77}$$

where z_* denotes the value of z at the turning point. This relation is valid also for the time-dependent case, as one can show in an analogous manner.

The boundary separation of the end points in vacuum can be found by solving (76) and reads

$$\ell = 2\int_0^{z_*} \frac{dz}{\sqrt{(\frac{z}{z_*})^{\theta-2}-1}}\,. \tag{78}$$

This can be written in a more transparent form by moving to a dimensionless variable $k = z/z_*$ with a fixed interval

$$\ell = 2z_* \int_0^1 dk (k^{\theta-2}-1)^{-1/2}\,. \tag{79}$$

The vacuum action is given by

$$S = 2{z_*}^{1-\theta/2} \int_0^{z_*} dz \frac{z^{\theta-2}}{\sqrt{(z/z_*)^{\theta-2}-1}} \tag{80}$$

which in terms of k reads

$$S = 2z_*^{\theta/2} \int_0^1 dk k^{\theta-2} (k^{\theta-2}-1)^{-1/2}\,. \tag{81}$$

This result enables us to find the vacuum correlator for different values of θ. For example for $\theta = 1$ we obtain

$$S = 2\sqrt{\pi\ell}\,. \tag{82}$$

The results can be normalized in a natural way by subtracting the vacuum value from the Vaidya result. Using this scheme has the nice feature of having zero value for the entropy before the quench. Other schemes also exist, as illustrated by the plots in paper [I]. These plots highlight the nontrivial and important role of choosing the regularization in constructing a holographic model of this kind.

3.6 Minimal surface

Following [24] we shall now investigate the minimal surfaces in the HLV geometry. As dicussed earlier, the area of a bulk surface hanging from the boundary of a region on the spacetime boundary is associated with the entanglement entropy of this boundary region. The boundary geometry chosen here is an infinite strip of width ℓ. For a infinite strip we can parametrize the hanging surface in a simple way by using the boundary coordinates x and y. We shall take the strip to be infinite in the y direction and have

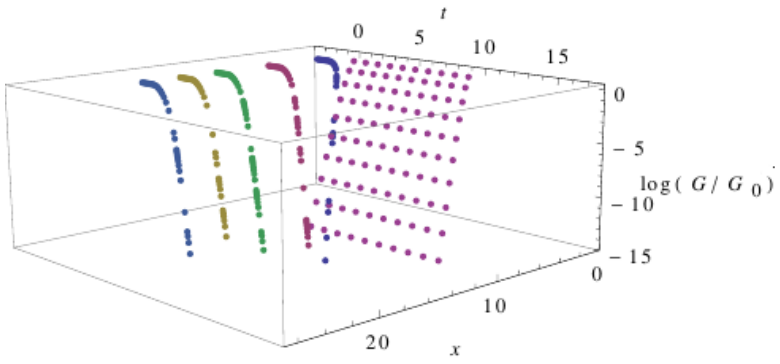

Figure 2: Sparse set of data triplets for the case $\zeta = 2$ and $\theta = 1$.

width ℓ in the x direction. Due to the symmetry in y we can take the coordinates to be functions of x only. The bulk surface thus resembles a very long sheet with its shorter egdes attached to two horizontal rods situated at $x_1 = -\ell/2$ and $x_2 = \ell/2$ at the boundary.

For concrete calculations we introduce the Eddington-Finkelstein coordinates on the surface and parametrize them in terms of x as in the geodesic case. By substituting the expressions

$$z = z(x), v = v(x) \tag{83}$$

we find the surface metric to be

$$ds^2 = (-z^{-2\zeta+\theta}b(z,v)(v')^2 - 2z^{-1-\zeta+\theta}v'z' + z^{-2+\theta})dx^2 + z^{-2+\theta}dy^2 \tag{84}$$

resulting in the surface action

$$S = \int dy \int dx \sqrt{(-z^{-2\zeta+\theta}b(z,v)(v')^2 - 2z^{-1-\zeta+\theta}v'z' + z^{-2+\theta})z^{-2+\theta}}\,. \tag{85}$$

Due to the infinite interval in y it is more convenient to study the entropy density

$$s = \frac{S}{\int dy}\,. \tag{86}$$

In the following we shall consider this scaled quantity while keeping in mind its structure.

In the strip case the action is again independent of x, which allows us to construct a conserved Hamiltonian

$$H = \frac{\partial L}{\partial z'}z' + \frac{\partial L}{\partial v'}v' - L = -\frac{1}{z^{4-2\theta}L}\,. \tag{87}$$

Using the turning point value

$$H = -z_*^{-2+\theta} \tag{88}$$

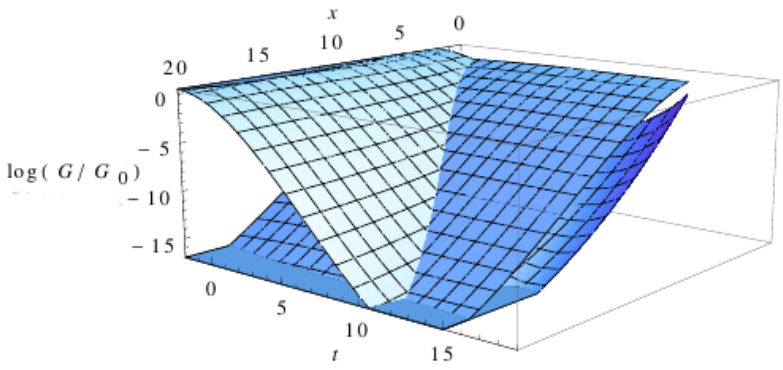

Figure 3: An example of a surface plot of the boundary distance and time versus geodesic length with vacuum value subtracted. The intersection of the two fitted surfaces corresponds to the transition from the time dependent solution to the thermal state, as discussed in the text.

we can use this to find the on-shell Lagrangian as

$$L = \frac{z^{-4+2\theta}}{z_*^{-2+\theta}} \,. \tag{89}$$

Doing a calculation in vacuum further yields the result

$$z_*^{\theta-2} = \frac{z^{\theta-2}}{\sqrt{1+(z')^2}} \,. \tag{90}$$

This can be cast in the form

$$z' = \sqrt{(\frac{z}{z_*})^{2\theta-4} - 1} = \frac{dz}{dx} \tag{91}$$

which gives the vacuum relation between z_* and l as

$$\ell = 2z_* \int_0^1 (k^{2\theta-4} - 1)^{-1/2} \,. \tag{92}$$

From the expression of L in terms of the turning point value z_* we can find the vacuum surface area or entanglement entropy to be

$$S = \int dx \frac{z^{-4+2\theta}}{z_*^{-2+\theta}} = 2z_*^{2-\theta} \int_0^{z_*} dz \frac{z^{-4+2\theta}}{\sqrt{(\frac{z}{z_*})^{2\theta-4} - 1}} \,. \tag{93}$$

By a change of variable this can be cast into the form

$$S = 2z_*^{\theta-1} \int_0^1 k^{2\theta-4} (k^{2\theta-4} - 1)^{-1/2} \,, \tag{94}$$

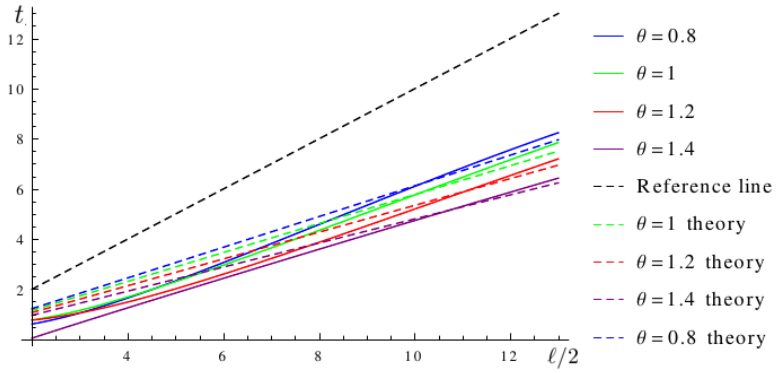

Figure 4: Plot of thermalisation time versus distance with different values of the hyperscaling exponent. The theoretically predicted constant speed of thermalization (102) for late times is given by the dashed line. The black dashed reference line has slope 1. Numerical artefacts are visible at small values of t.

which tells us that S only depends on z_*. This result has great significance in numerical calculations. By adjusting the vacuum solution to the value of z_* with the same endpoints, we can find the vacuum value of the action.

3.7 Entanglement results

We can calculate the surface area and finishing time at the boundary as a function of strip width for hanging surfaces with different turning point coordinates in the bulk. According to the area-entropy duality these values will correspond to the entanglement entropy associated with the strip at different times and its thermalization in the dual theory.

The equations of motion can be found from the action with metric (84). The two Lagrange equations can be again combined to obtain

$$zv'' + 4(1-\frac{\theta}{2})z'v' - 2(1-\frac{\theta}{2})z^{-1+\zeta} + (1+\zeta-\theta)z^{1-\zeta}v'^2 - \frac{\zeta-\theta}{2}z^{3-\theta}m(v)v'^2 = 0\,. \quad (95)$$

The other equation is given by the conserved Hamiltonian

$$-z^{2-2\zeta}b(z,v)v'^2 - 2z^{1-\zeta}v'z' + 1 = \frac{z_*^{4-2\theta}}{z^{4-2\theta}}\,. \quad (96)$$

The equations of motion are solved similarily to the geodesic case. We set the initial conditions with zero derivatives at the turning point $x = 0$ and solve these equations for different values of turning point radius and time numerically. As in the geodesic case, we will set values of z at the turning point to suitable values for each of the hyperscaling exponents and change the turning point time in diminishing steps. This results in data

triplets consisting of the strip width, boundary time and entanglement entropy of the strip. A similarly modified procedure with turning point outside the horizon is performed for the thermalized case. The results are normalized by subtracting the vacuum result, which gives us zero entanglement entropy before the quench. The results are regulated by stopping the integration slightly before reaching the boundary. The data triplets for dynamic and thermalized surfaces are plotted together, which results in a figure similar to 5. As in the geodesic case, the results are insensitive to the specific form of the quench as long as the shell is reasonably thin.

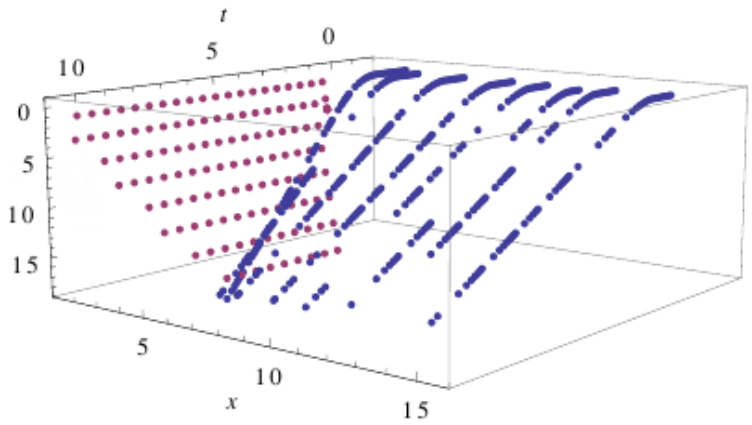

Figure 5: Set of data points for entaglement entropy density as a function of strip half-width and time.

We can also investigate the famous linear growth of the entanglement entropy before thermalization by fitting a linear function to the points in the appropriate regime. This was done with various values of ζ and θ, which produces the results plotted in figure 6. The time development of entanglement entropy can also be compared to the analytical predictions of chapter 3.8 plotted in the same figure. The agreement is fairly good, if one takes into account the inaccuracies of the fitting process. One should also note that the overall vertical range is quite small in this plot.

We can investigate one of the points more carefully and plot the actual data points for one of the parameter pairs. In figure 7 we have chosen the values $\theta = 1$ and $\zeta = 2$ and plotted two of the data sets.

The time development can be seen even more clearly by flattening plot 7 in the x-direction. The resulting figure 8 shows the initial growth followed by a linear regime.

We can also pick the data set around $x = 8$, although this is not absolutely necessary due to the invariance in x. The corresponding plot 9 also shows the structure of the data set more clearly.

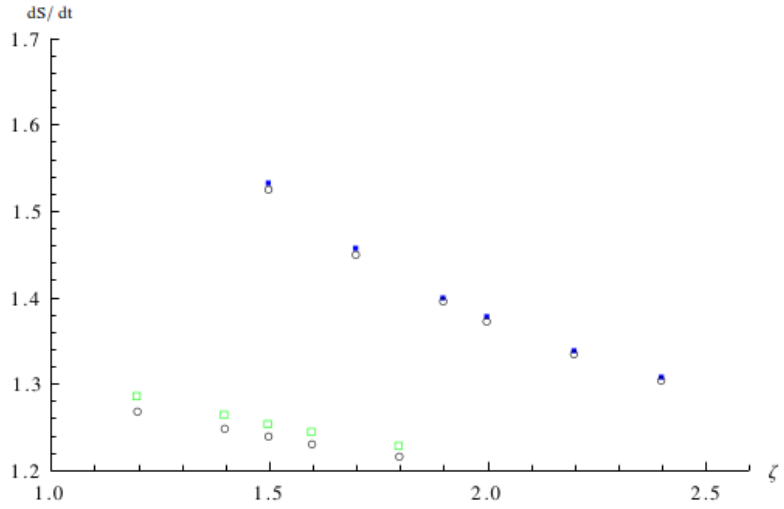

Figure 6: Linear regime for the strip: the colored squares are values of the slope found from the numerical data similar to figure 5 with chosen flattened sequences analogous to figure 8. The black empty circles denote the analytical predictions of section 3.8. Upper set of points corresponds to $\theta = 1$ and lower to $\theta = -0.5$.

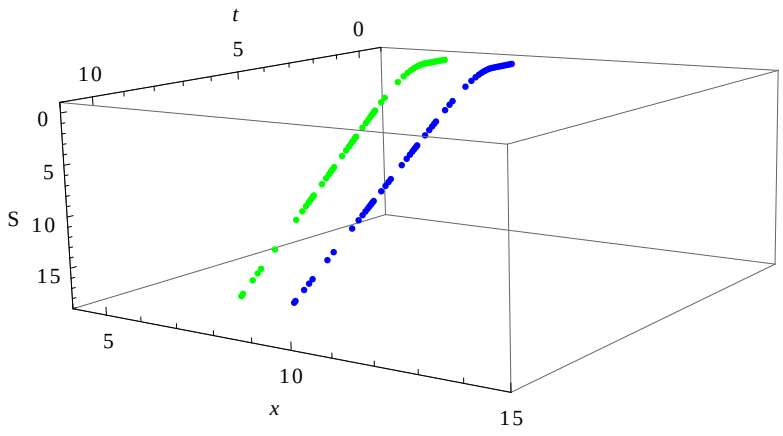

Figure 7: Two sets of data points in the case $\theta = 1$ and $\zeta = 2$.

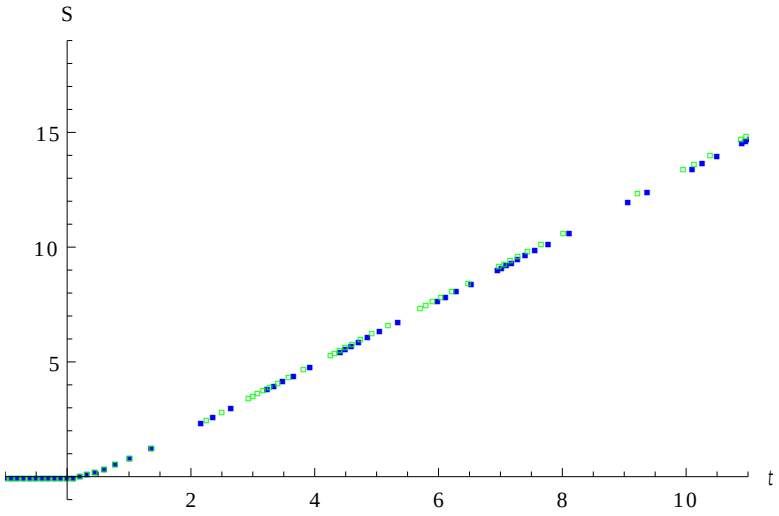

Figure 8: The two sets of data points in the case $\theta = 1$ and $\zeta = 2$ flattened. The slope seems to be rather independent of x, as predicted by theory.

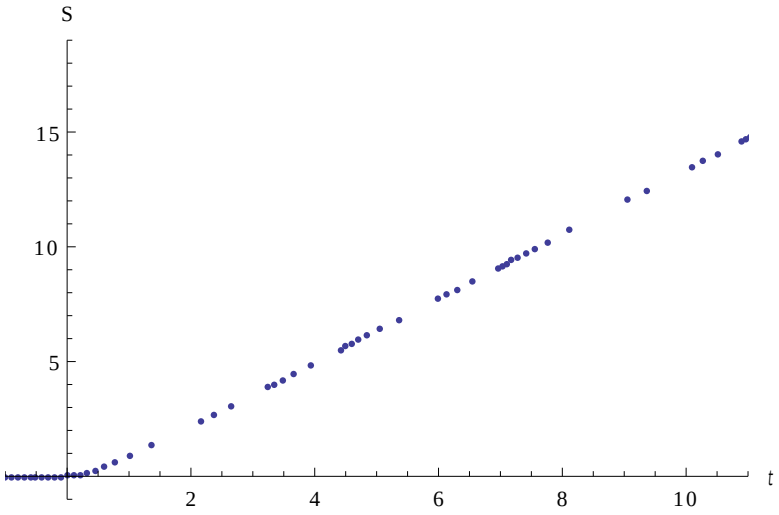

Figure 9: The data set around $x = 8$ flattened.

The s/t-ratio as a function of time is plotted in figure 10. The overall entanglement entropy linearizes quite fast despite the non-linear initial growth.

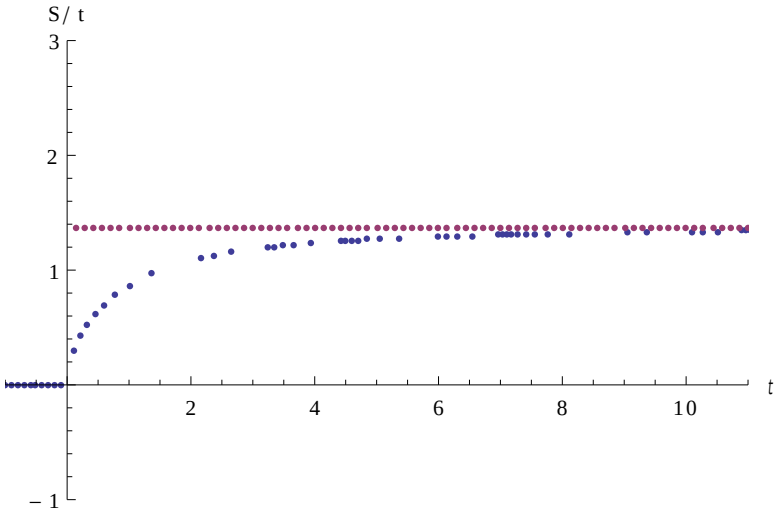

Figure 10: The s/t-ratio of the plot 9 as a function of t. The pink line is the analytic prediction for the linear regime.

Figure 8 shows that the agreement is equally good for the combination of two data sets with x-separation, as expected.

3.8 Linear behaviour

At late times, the growth rate of entanglement entropy linearizes. In absence of hyperscaling violation the phenomenon was investigated by Liu and Suh in their two papers [36] and [37]. Based on their results, the relevant formulas for the most general case with both Lifshitz scaling and hyperscaling violation were derived in article [I]. In the thin shell regime one finds

$$\ell_\perp^{d-1} s = \mathcal{A}^{(3)}_{\rm reg}(t) = 2\ell_\perp^{d-1} A^{(3)}_{\rm reg}(t)\,, \qquad A^{(3)}_{\rm reg}(t) = \frac{\sqrt{-F(z_m)}}{z_m^{d_\theta+\zeta-1}}\, t \equiv \frac{v_E}{z_h^{d_\theta+\zeta-1}}\, t, \tag{97}$$

where $F(z)$ is the mass function and z_m is the minimal point of z'^2. Here we set the horizon distance $z_h = 1$.

For the HLV metric the growth rate of entanglement entropy v_E is

$$v_E = \frac{(\kappa-1)^{\frac{\kappa-1}{2}}}{\kappa^{\frac{\kappa}{2}}}\,, \qquad \kappa = \frac{2(d_\theta+\zeta-1)}{d_\theta+\zeta}\,. \tag{98}$$

Plots 8-11 show that this result agrees with the numerical calculation with good accuracy.

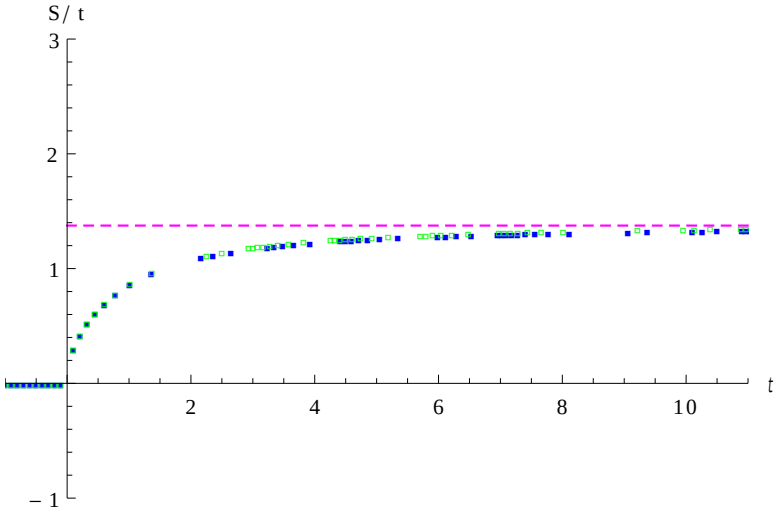

Figure 11: The s/t-ratio of the plot 8 as a function of t. The pink line is the analytic prediction for the linear regime.

Also other predictions of Liu and Suh were generalized and compared to the numerics in paper [I]. The initial non-linear behaviour of entanglement entropy is of the form

$$\mathcal{A}^{(3)}_{\text{reg}}(t) = \frac{M A_\Sigma \, \zeta^{1+1/\zeta}}{2(\zeta+1)} \, t^{1+1/\zeta} \,, \tag{99}$$

where M denotes the mass of the shell and Σ is the boundary of the entangling region. This formula agrees with numerical results obtained in our paper, which also confirms that the result is independent of θ as expected.

The speed of thermalization ℓ/t_s will also linearize at late times. At leading order, entanglement entropy reaches the thermal value in time

$$t_s = z_h^{\zeta-1} \sqrt{\frac{d_\theta}{2 z_h F_h'}} \, \ell \,. \tag{100}$$

The result depends on the boundary dimension. If the boundary is a "strip" of dimension n, thermalization occurs at

$$t_s = z_h^{\zeta-1} \sqrt{\frac{n d_\theta}{2 d z_h F_h'}} \, \ell + \dots \,. \tag{101}$$

For entanglement entropy $n = d$ and we obtain the result given above. Geodesics correspond to a line, so the boundary has dimension 1 and the boundary of the boundary

consists of the two endpoints. Geodesics thus thermalize at

$$t_s = z_h^{\zeta-1}\sqrt{\frac{d_\theta}{2dz_hF_h'}}\,\ell + \dots\ . \tag{102}$$

This prediction was tested against geodesic data in figure 4, which shows the asymptotic linearization of thermalization velocity.

As the final draft was being written, Alishahiha et al published a third article [29] with partial overlap with our results. The analytic results are derived for the case $d_\theta \geqslant 2-\zeta$. It is worth noting that parts of the parameter space outside this region have a negative effective dimension if one wants to satisfy the null energy condition. This causes both calculational and conceptual problems.

4 Heavy ion collisions and Holographic QGP

In recent years, heavy ion collisions have been an important way of studying nuclear matter. In addition to its main task, finding the Higgs boson, the LHC collider at CERN accelerated lead ions to investigate the structure of matter at unprecedented energies. These processes had been previously studied at lower energies by using the RHIC facility in the US. In these energetic collisions a new state of matter called Quark Gluon Plasma (QGP) is created. This state of matter is analogous to ordinary plasma, in which the temperature is high enough to dissociate atoms to form a mixture of free nuclei and electrons. In QGP, however, nuclei themselves get ripped apart and even protons and neutrons dissolve into a mixture of quarks and gluons.

This state of matter has interesting properties, one of which is its very rapid thermalization after its creation. Experiments at RHIC and at the LHC have shown that the plasma starts to behave in a collective way at very early stages of the process. This means that the plasma is strongly coupled, which, of course, is not very surprising. These heavy ion experiments are thus one of the few ways of experimentally studying thermalization in a strongly coupled gauge theory.

This kind of quantum fluid is thus both interesting and difficult to study. Various semi-phenomenological models have been developed to model and understand the thermalization and anisotropies of this state of matter. The most established ones are viscous hydrodynamics [38] and free streaming. Both of these are used in modelling the phenomena, although they are classically not expected to capture the dynamics of the system. One of the interesting aspects is the very early applicability of hydrodynamics which is usually thought to be a low energy description for equilibrated matter. There exists many holographic studies on quantum fluids and QGP. Many of these have been very successful in explaining various aspects of the dynamics. One of the most famous results is the very low shear viscosity [39] of these fluids. The values obtained from holographic models (e.g. [40], [41], [42]) are close to the actual measurements done on heavy ion collisions.

In the two papers [II]and [III] we tackled this problem by using the framework of gauge/gravity correspondence. Our main goal was to study inhomogeneous initial states and their behaviour. This work is an important generalization of the previously investigated holographic models, such as [43] with homogeneous and isotropic injection of energy or boost invariant plasmas [44] with rotational and translational symmetry.

The thermalizing plasma was modelled by an infalling scalar field in an anti-de-Sitter background. The scalar field will collapse to form a black brane, which corresponds to thermalization in the field theory side. This model has the additional advantage of being analytically solvable, which is not the case with the other holographic models, such as colliding shockwaves [45, 46] and [47] or boost invariant plasmas [48],[49] where numerical general relativity is needed.

Our approach is a generalization of the procedure used in [43], which in turn has roots in earlier papers. The authors themseves refer to Chesler and Yaffe [50] and even earlier

papers, like [51], arguably contained some of the ingredients. In this model we turn on a Gaussian scalar source at the boundary of pure AdS space. This source acts as a boundary condition for the gravity solution. To investigate the effect of fluctuations in the initial state, we will make the source inhomogeneous in one of the transverse directions.

The first task is to solve the Einstein equations for this situation and obtain the metric. Following [43], we used an expansion in the small amplitude of the scalar fields and tried to solve the equations order by order. This turned out to be the hardest part of the work, as spatial derivatives introduced by the transverse inhomogeneity made the solution process more tedious than expected. Several different techniques were tried in order to solve the general form of the field equations. The solution was finally obtained by assuming the length scale of the inhomogeneity to be large and using a cleverly arranged double expansion in both the initial field and spatial derivatives.

The following task was to extract the boundary dynamics from the solution. This was done by using the Fefferman-Graham expansion, which allows one to read out the boundary stress tensor in a straightforward way, see [52]. Extracting the fluid dynamics of QGP from the stress tensor requires one to boost the solution into the local rest frame. Comparing the results to the established models used in the heavy ion community is not trivial, as one has to fix the corresponding conditions for these models. In the case of viscous hydrodynamics, we can use the local velocity as our input. In the free streaming case one injects a stream of non-interacting null dust with the same energy distribution.

The results given by these scenarios can then be compared to the ones predicted by AdS/CFT. In the case of pressure anisotropy, we find good agreement with the established models. The two phenomenological models do not agree at early times, but the holographic picture seems to follow the relevant ones in different phases of the thermalization. In the early stages hydrodynamics is not relevant, as the plasma has not had enough time to hydrodynamize. In the later stages all three models behave similarly. This result can be used to justify the early use of minimal viscous hydrodynamics in modelling strongly coupled plasmas. The calculations generalize the previous investigations by adding inhomogeneity to the initial conditions and prove the applicability of the Gauge/Gravity duality in this kind of more realistic situation.

4.1 Holographic model

The gravity side consists of a collapsing shell of massless scalars in a (3+1)-dimensional AdS-space. From the action

$$S = \frac{1}{16\pi G_N} \int d^{d+1}x\sqrt{g}\left(R - 2\Lambda - \frac{1}{2}g^{\mu\nu}\partial_\mu\phi\partial_\nu\phi\right) \tag{103}$$

with

$$\Lambda = -\frac{d(d-1)}{2} = -3 \tag{104}$$

we derive the equations of motion

$$E_{\mu\nu} \equiv G_{\mu\nu} - \frac{1}{2}\partial_\mu\phi\partial_\nu\phi + g_{\mu\nu}\left(-3 + \frac{1}{4}(\partial\phi)^2\right) = 0 \qquad (105)$$
$$\Box\phi = \frac{1}{\sqrt{g}}\partial_\mu\left(\sqrt{g}g^{\mu\nu}\partial_\nu\phi\right) = 0\,.$$

The scalar shell is created by setting the initial value of the field to be nonzero at the boundary, which is located at $r \to \infty$. The equations of motion are solved and corresponding energy-momentum tensor at the boundary calculated. By boosting this to the local rest frame we obtain a fluid-like form, from which the hydrodynamics of the Quark Gluon Plasma can be extracted by using the conventional interpretation. We have chosen the dimension (3+1) to have the necessary amount of transverse directions with an odd number of spatial dimensions in the bulk. In odd dimensions the isotropic solution does not contain transcendental functions, as is the case in even dimensions.

4.2 Anisotropic case

The first task is to solve the dynamics from the equations of motion in the anisotropic case. This was first tried by straightforward substitution. The x-dependent metric Ansatz

$$\begin{aligned} ds^2 &= -h(v,r,x)dv^2 + 2dv(dr + k(v,r,x)dx) + \\ &+ f(v,r,x)^2 e^{B(v,r,x)}dx^2 + f(v,r,x)^2 e^{-B(v,r,x)}dy^2 \\ \phi &= \phi(v,r,x) \end{aligned} \qquad (106)$$

was substituted into the equations of motion and the resulting equations fed to the suitable solving routines. In spite of trying several combinations with the assumption of small source with an even smaller anisotropy these equations turned out to be too hard to solve analytically this way. The assumption of slow spatial dependence and expansion in derivatives with respect to x was first introduced in this phase, but alone it did not suffice. Separating the spatial dependence and trying a wide range of ideas was, however, quite useful in the later group discussions about possible solving techniques. At the same time other members of the group tried to solve the original equations by using propagators. Despite the initial successes in reproducing previous results, the inhomogeneous case proved out to be too complicated. The solution was finally obtained by using a double gradient expansion in the two parameters. The solution progresses separately in orders of ϵ and μ, which express the order of expansion in the scalar field and spatial derivative, respectively. The unknown functions in (106) are thus expressed

as double expansions

$$\begin{aligned} h(v,r,x) &= \sum_{n,i=0}^{\infty} \epsilon^n \mu^i h_{n,i}(v,r,\mu x) & k(v,r,x) &= \sum_{n,i=0}^{\infty} \epsilon^n \mu^i k_{n,i}(v,r,\mu x) \\ f(v,r,x) &= \sum_{n,i=0}^{\infty} \epsilon^n \mu^i f_{n,i}(v,r,\mu x) & B(v,r,x) &= \sum_{n,i=0}^{\infty} \epsilon^n \mu^i b_{n,i}(v,r,\mu x) \\ \phi(v,r,x) &= \sum_{n,i=0}^{\infty} \epsilon^n \mu^i \phi_{n,i}(v,r,\mu x)\,. \end{aligned} \tag{107}$$

and the equations of motion are solved order by order with the boundary condition set by the scalar source

$$\begin{aligned} &\varphi(v,\mu x) = 0 && v \leq 0 \\ &\varphi(v,\mu x) = \epsilon \varphi_0(v,\mu x) && 0 < v < \delta t \\ &\varphi(v,\mu x) = 0 && v \geq \delta t\,. \end{aligned} \tag{108}$$

We also require the metric to be purely AdS before the injection and remain asymptotically AdS after the injection.

It turns out to be easier to work with conveniently chosen linear combinations of the equations instead of the original ones coming straight from the Lagrangian. These equations are then solved up to second order in ϵ and fourth order in μ. The final result is is of the form

$$\begin{aligned} h(v,r,x) &= r^2 \left(1 + \frac{\mathcal{H}_{(2)}}{r^2} + \frac{\mathcal{H}_{(3)}}{r^3} + \frac{\mathcal{H}_{(4)}}{r^4}\right) + O\left(\epsilon^3, \mu^5\right) \\ f(v,r,x) &= r + \frac{\mathcal{F}_{(1)}}{r} + \frac{\mathcal{F}_{(2)}}{r^2} + \frac{\mathcal{F}_{(3)}}{r^3} + O\left(\epsilon^3, \mu^5\right) \\ k(v,r,x) &= \mathcal{K}_{(0)} + \frac{\mathcal{K}_{(1)}}{r} + O\left(\epsilon^3, \mu^5\right) \\ B(v,r,x) &= \frac{\mathcal{B}_{(2)}}{r^2} + \frac{\mathcal{B}_{(3)}}{r^3} + \frac{\mathcal{B}_{(4)}}{r^4} + O\left(\epsilon^3, \mu^5\right) \end{aligned} \tag{109}$$

$$\phi(v,r,x) = \Psi_{(0)} + \frac{\Psi_{(1)}}{r} + \frac{\Psi_{(2)}}{r^2} + \frac{\Psi_{(3)}}{r^3} + O\left(\epsilon^3, \mu^5\right)\,, \tag{110}$$

where the coefficients have rather complicated but elementary expressions in terms of the boundary source, as shown in paper [III]. By setting spatial derivatives to zero one recovers the isotropic solution of [43].

It is worth noting that the preceding calculation is based on a two-parameter expansion around pure AdS-space. This naive perturbation theory, as it is called by Bhattcharyya and Minwalla, is valid only at short timescales. Investigating the late-time dynamics reliably would require resummed perturbation theory in which the expansion is carried out in AdS-Vaidya background. The regime of validity of naive perturbation theory was

investigated more thoroughly in [43] where it was found that the perturbative approach around AdS is reliable if $t \ll 1/T$.

In the isotropic case the metric after the injection has the AdS-Vaidya form

$$ds^2 = -\left(r^2 - \frac{M(v)}{r}\right) dv^2 + 2dvdr + r^2(dx^2 + dy^2)\,. \tag{111}$$

By analogy, we define the mass function $M(v)$ to be the coefficient of the $1/r$-term in $h(v, r, x)$. Similarly to the isotropic case, we find the relation $T \propto M^{1/3} \propto \frac{\epsilon^{2/3}}{\delta t}$.

In the μ-expansion the anisotropy in x is assumed to be gentle enough to allow an expansion in the spatial derivatives. According to the considerations above, the natural scale of the problem is given by the inverse temperature. We can thus assume the second expansion to be valid provided that the length scale of spatial variations λ is much larger than $1/T$, which also guarantees the leading behaviour of the mass to be of the assumed form. The results of the perturbative calculation are thus applicable as long as $t \ll 1/T \ll \lambda$ where λ is governed by the first expansion parameter and injection time.

4.3 Fefferman-Graham expansion and boundary dynamics

One of the main advantages of AdS-space, in addition to flat boundary, is that there exists a very straightforward method for extracting the asymptotic form of the stress tensor from the bulk metric. The method presented in [52] is nowadays widely used in holographic calculations. The procedure begins with the Gibbons-Hawking boundary term containing exterior curvature of the boundary and using the renormalization scheme to get rid of the divergences. This procedure connects the asymptotic form of the metric to the boundary stress tensor. Simply by transforming the metric into the form

$$ds^2 = \frac{d\rho^2}{\rho^2} + \rho^2 g_{\alpha\beta}(t, \rho, \chi) dx^\alpha dx^\beta \tag{112}$$

where

$$g_{\alpha\beta}(t, \rho, \chi) = g(0)_{\alpha\beta}(t, \chi) + \frac{g(2)_{\alpha\beta}(t, \chi)}{\rho^2} + \frac{g(3)_{\alpha\beta}(t, \chi)}{\rho^3} + \ldots, \tag{113}$$

we can obtain the stress energy tensor at the boundary $\rho \to \infty$ as

$$\langle T_{\alpha\beta} \rangle = \frac{3}{16\pi G_N} g(3)_{\alpha\beta}\,. \tag{114}$$

In practice, the coefficients were found by finding a asymptotic coordinate transform that brings the metric into the desired form up to suitably high order in the inverse radius.

The next step is thus to find the form of the obtained metric in Fefferman-Graham coordinates and extract the boundary dynamics. These calculations were carried out for a arbitrary boundary source for maximal generality and easier interpretation of the

results. As previously mentioned, we did not search for an exact coordinate transform, as we do not need the higher terms in the series. By using the asymptotic transform

$$\begin{aligned} v &\approx t - \frac{1}{\varrho} + \frac{v_3}{\varrho^3} + O(\varrho^{-4}) \\ r &\approx \varrho\left(1 - \frac{\mathcal{H}_{(2)} - 3v_3}{3\varrho^2} + \frac{r_3}{\varrho^3} + O(\varrho^{-4})\right) \\ x &\approx \chi + \frac{\mathcal{K}_{(0)}}{3\varrho^3} + O(\varrho^{-4}) \end{aligned} \tag{115}$$

with

$$v_3 = \frac{1}{12}\mathcal{H}_{(2)} \tag{116}$$

and

$$r_3 = -\frac{1}{6}\left(\mathcal{H}_{(3)} + 4\mathcal{F}_{(2)} - 4\dot{\mathcal{F}}_{(1)} - \frac{1}{3}\dot{\mathcal{H}}_{(2)} + \frac{2}{3}\mathcal{K}'_{(0)}\right) \tag{117}$$

we obtain the desired term $g_{(3),\alpha\beta}$ as

$$g_{(3),\alpha\beta} = \frac{1}{3} \times$$

$$\begin{pmatrix} -2\mathcal{H}_{(3)} & -\mathcal{H}'_{(2)} - 2\dot{\mathcal{K}}_{(0)} + 3\mathcal{K}_{(1)} & 0 \\ -\mathcal{H}'_{(2)} - 2\dot{\mathcal{K}}_{(0)} + 3\mathcal{K}_{(1)} & -\mathcal{H}_{(3)} - 3\mathcal{B}_{(3)} + 3\dot{\mathcal{B}}_{(2)} + \mathcal{K}'_{(0)} & 0 \\ 0 & 0 & -\mathcal{H}_{(3)} + 3\mathcal{B}_{(3)} - 3\dot{\mathcal{B}}_{(2)} - \mathcal{K}'_{(0)} \end{pmatrix}, \tag{118}$$

where spatial derivatives are denoted by a comma and temporal derivatives by a dot.

The stress tensor at the boundary thus has the components

$$\begin{aligned} T_{tt} &= -\frac{2}{16\pi G_N}\mathcal{H}_{(3)} \\ T_{xx} &= -\frac{1}{16\pi G_N}\left(\mathcal{H}_{(3)} - 3\mathcal{B}_{(3)} + 3\dot{\mathcal{B}}_{(2)} - \mathcal{K}'_{(0)}\right) \\ T_{tx} &= -\frac{1}{16\pi G_N}\left(\mathcal{H}'_{(2)} + 2\dot{\mathcal{K}}_{(0)} - 3\mathcal{K}_{(1)}\right) \\ T_{yy} &= -\frac{1}{16\pi G_N}\left(\mathcal{H}_{(3)} + 3\mathcal{B}_{(3)} - 3\dot{\mathcal{B}}_{(2)} + \mathcal{K}'_{(0)}\right). \end{aligned} \tag{119}$$

In order to get numerical results, one has to express the relevant elements of this tensor in terms of derivatives and integrals of the boundary source. This stage was algebraically quite demanding, so calculations were cross-checked carefully by two people.

For the time-time component we obtain the explicit result

$$
\begin{aligned}
T_{tt} \;=\; & -\frac{1}{16\pi G_N}\Bigg\{\frac{1}{2}\int_{-\infty}^{t} d\tau\ \Bigg[2\dot{\varphi}(\tau,x)\dddot{\varphi}(\tau,x) - \left(\ddot{\varphi}'(\tau,x)\right)^2 \\
& -4\dot{\varphi}(\tau,x)\dot{\varphi}''(\tau,x) + 2\ddot{\varphi}(\tau,x)\varphi''(\tau,x) + 2\ddot{\varphi}'(\tau,x)\varphi'(\tau,x) \\
& +2\frac{\partial}{\partial x}\int_{-\infty}^{\tau} ds\ \left[\dot{\varphi}(s,x)\ddot{\varphi}'(s,x) - \int_{-\infty}^{s} dw\ \ddot{\varphi}'(w,x)\ddot{\varphi}(w,x)\right]\Bigg] \\
& -\frac{1}{2}\int_{-\infty}^{t} d\tau\ \left[(\varphi''(\tau,x))^2 + \varphi'(\tau,x)\varphi'''(\tau,x)\right] \\
& +\frac{3}{8}\int_{-\infty}^{t} d\tau\dot{\varphi}(\tau,x)\int_{-\infty}^{\tau} ds\ \varphi''''(s,x) \\
& -\frac{1}{2}\frac{\partial}{\partial x}\int_{-\infty}^{t} d\tau\int_{-\infty}^{\tau} ds\ \left[\dot{\varphi}(s,x)\varphi'''(s,x) - 2\dot{\varphi}'(s,x)\varphi''(s,x)\right] \\
& +\frac{1}{4}\frac{\partial^2}{\partial x^2}\int_{-\infty}^{t} d\tau\int_{-\infty}^{\tau} ds\int_{-\infty}^{s} d\omega\ \Bigg[-\frac{5}{2}(\dot{\varphi}'(\omega,x))^2 - 4\dot{\varphi}(\omega,x)\dot{\varphi}''(\omega,x) \\
& \qquad +2\ddot{\varphi}(\omega,x)\varphi''(\omega,x) + 2\ddot{\varphi}'(\omega,x)\varphi'(\omega,x)\Bigg] \\
& +\frac{3}{4}\frac{\partial^3}{\partial x^3}\int_{-\infty}^{t} d\tau\int_{-\infty}^{\tau} ds\int_{-\infty}^{s} d\omega\int_{-\infty}^{\omega} dp\int_{-\infty}^{p} dq\ \dot{\varphi}(q,x)\dddot{\varphi}'(q,x)\Bigg\}.
\end{aligned}
\tag{120}
$$

4.4 The dual theory and QGP results

In the actual modelling stage we assumed that the spatial and temporal parts are independent i.e. that the boundary source can be written as

$$
\varphi(t,x) = u(x)\varphi_0(t)\,, \tag{121}
$$

and the temporal part has a finite support

$$
\begin{array}{ll}
\varphi_0(t) = 0\,, & t \le 0 \\
\varphi_0(t) = \epsilon\tilde{\varphi}_0(t)\,, & 0 < t < \delta t \\
\varphi_0(t) = 0\,, & t \ge \delta t
\end{array}
\tag{122}
$$

as assumed in the derivation of the gradient series. Using this Ansatz, we can write the metric components in a more illuminating form. By using integration by parts and

collecting terms the time-time component becomes

$$\begin{aligned}
T_{tt} \;=\; & -\frac{1}{16\pi G_N}\Bigg\{u(x)^2\int_{-\infty}^{t}d\tau\ \dot\varphi_0(\tau)\dddot\varphi_0(\tau)\\
& -\frac{1}{2}\Big[u'(x)^2+4u(x)u''(x)\Big]\int_{-\infty}^{t}d\tau\ \left(\dot\varphi_0(\tau)\right)^2\\
& +\frac{1}{2}\frac{\partial^2}{\partial x^2}u(x)^2\int_{-\infty}^{t}d\tau\ \ddot\varphi_0(\tau)\varphi_0(\tau)\\
& +\frac{1}{2}\frac{\partial^2}{\partial x^2}u(x)^2\int_{-\infty}^{t}d\tau\int_{-\infty}^{\tau}ds\int_{-\infty}^{s}dw\ \dot\varphi_0(w)\dddot\varphi_0(w)\\
& +\frac{3}{8}u(x)u''''(x)\int_{-\infty}^{t}d\tau\ \dot\varphi_0(\tau)\int_{-\infty}^{\tau}ds\ \varphi_0(s)\\
& -\frac{1}{8}\frac{\partial}{\partial x}\Big[9u'(x)u''(x)+6u(x)u'''(x)\Big]\int_{-\infty}^{t}d\tau\ \varphi_0(\tau)^2\\
& +\frac{3}{8}\frac{\partial^2}{\partial x^2}\Big[3(u'(x))^2+4u(x)u''(x)\Big]\int_{-\infty}^{t}d\tau\int_{-\infty}^{\tau}ds\int_{-\infty}^{s}d\omega\ \varphi_0(\omega)\ddot\varphi_0(\omega)\\
& +\ \frac{3}{8}\frac{\partial^4}{\partial x^4}u(x)^2\int_{-\infty}^{t}d\tau\int_{-\infty}^{\tau}ds\int_{-\infty}^{s}d\omega\int_{-\infty}^{\omega}dp\int_{-\infty}^{p}dq\ \dot\varphi_0(\omega)\dddot\varphi_0(\omega)\Bigg]\Bigg\}\ .
\end{aligned}\tag{123}$$

The true advantage of separating the temporal and spatial dependence is that we can express the components in the form

$$\begin{aligned}
T_{tt} =& \frac{1}{16\pi G_N}\Bigg\{u(x)^2A(t)+\frac{1}{2}\frac{\partial^2}{\partial x^2}u(x)^2C(t)+\frac{1}{2}\frac{\partial^2}{\partial x^2}u(x)^2D(t)\\
& -\frac{1}{2}\left(u'(x)^2+4u(x)u''(x)\right)E(t)\\
& -\frac{1}{8}\frac{\partial}{\partial x}\left(9u'(x)u''(x)+6u(x)u'''(x)\right)F(t)+\frac{3}{8}u(x)u''''(x)G(t)\\
& +\frac{3}{8}\frac{\partial^2}{\partial x^2}\left(3(u'(x))^2+4u(x)u''(x)\right)H(t)+\frac{3}{8}\frac{\partial^4}{\partial x^4}u(x)^2J(t)\Bigg\}\ .
\end{aligned}\tag{124}$$

Using our assumption of a finite temporal support for the energy injection, we can write the unknown functions as

$$
\begin{aligned}
A(t) &= \begin{cases} \bar{A} = -\int_{-\infty}^{\delta t} d\tau\ \dot{\varphi}_0(\tau)\dddot{\varphi}_0(\tau) = \text{const} & t > \delta t \\ \alpha(t) = -\int_{-\infty}^{t} d\tau\ \dot{\varphi}_0(\tau)\dddot{\varphi}_0(\tau) & t < \delta t \end{cases} \\
C(t) &= \begin{cases} \bar{C} + (t-\delta t)\bar{B} + \frac{1}{2}(t^2 - \delta t^2)\bar{A} & t > \delta t \\ \gamma(t) = \int_{-\infty}^{t} d\tau \int_{-\infty}^{\tau} dw\ \alpha(w) & t < \delta t \end{cases} \\
D(t) &= \begin{cases} \bar{D} = -\int_{-\infty}^{\delta t} d\tau\ \ddot{\varphi}_0(\tau)\varphi_0(\tau) = \text{const} & t > \delta t \\ \Delta(t) = -\int_{-\infty}^{t} d\tau\ \ddot{\varphi}_0(\tau)\varphi_0(\tau) & t < \delta t \end{cases} \\
E(t) &= \begin{cases} \bar{E} = -\int_{-\infty}^{\delta t} d\tau\ \left(\dot{\varphi}_0(\tau)\right)^2 = -\bar{D} & t > \delta t \\ \Upsilon(t) = -\int_{-\infty}^{t} d\tau\ \left(\dot{\varphi}_0(\tau)\right)^2 & t < \delta t \end{cases}
\end{aligned}
\tag{125}
$$

with

$$
\begin{aligned}
\bar{B} &= \int_{-\infty}^{\delta t} d\tau\ \alpha(\tau) \\
\bar{C} &= \gamma(\delta t) = \int_{-\infty}^{\delta t} d\tau \int_{-\infty}^{\tau} dw\ \alpha(w)
\end{aligned}
\tag{126}
$$

and

$$
\begin{aligned}
F(t) &= -\int_{-\infty}^{t} d\tau\ \varphi_0(\tau)^2 \\
G(t) &= -\int_{-\infty}^{t} d\tau\ \dot{\varphi}_0(\tau) \int_{-\infty}^{\tau} ds \varphi_0(s)\,.
\end{aligned}
\tag{127}
$$

One can easily notice that the latter become constant for $t > \delta t$. Following the convention set above, these constant values are denoted by $\bar{F}$ and $\bar{G}$.

The other factors

$$
\begin{aligned}
H(t) &= -\int_{-\infty}^{t} d\tau \int_{-\infty}^{\tau} ds \int_{-\infty}^{s} d\omega\ \varphi_0(\omega)\ddot{\varphi}_0(\omega) \\
J(t) &= -\int_{-\infty}^{t} d\tau \int_{-\infty}^{\tau} ds \int_{-\infty}^{s} d\omega \int_{-\infty}^{\omega} dp \int_{-\infty}^{p} dq\ \dot{\varphi}_0(q)\dddot{\varphi}_0(q)
\end{aligned}
\tag{128}
$$

will have a simple polynomial form at late times.

When all the energy has been injected, the boundary field becomes zero and we have

$$\begin{aligned} T_{tt}^{(t>\delta t)} = \frac{1}{16\pi G_N}\Bigg\{ & u(x)^2\bar{A} + \frac{1}{2}\frac{\partial^2}{\partial x^2}u(x)^2\left(\bar{C} + (t-\delta t)\bar{B} + \frac{1}{2}(t^2-\delta t^2)\bar{A}\right) \\ & + \frac{1}{2}\left(3(u'(x))^2 + 2u(x)u''(x)\right)\bar{D} \\ & + \frac{1}{8}\Bigg[-\frac{\partial}{\partial x}\left(9u'(x)u''(x) + 6u(x)u'''(x)\right)\bar{F} + 3u(x)u''''(x)\bar{G} \\ & + 3\frac{\partial^2}{\partial x^2}\left(3(u'(x))^2 + 4u(x)u''(x)\right)\left(\bar{H} + (t-\delta t)\bar{I} + (t^2-\delta t^2)\frac{\bar{D}}{2}\right) \\ & + 3\frac{\partial^4}{\partial x^4}u(x)^2\left(\bar{J} + (t-\delta t)\bar{K} + (t^2-\delta t^2)\frac{\bar{C}}{2} + (t^3-\delta t^3)\frac{\bar{B}}{6} + (t^4-\delta t^4)\frac{\bar{A}}{24}\right)\Bigg]\Bigg\}\,, \end{aligned} \tag{129}$$

which has a polynomial time dependence due to nested integrals in time. The barred constants are defined by integrals over the whole temporal support of the boundary source. With a similar kind of procedure one can derive the corresponding expressions for all components of the energy momentum tensor.

The EM-tensor obtained is easier to interpret if we move to the local rest frame of the fluid. In this frame the energy-momentum tensor is diagonal and reads $T^{\alpha\beta} = \mathrm{diag}(\varepsilon, p_x, p_y)$. The relation can be derived by boosting the diagonal form with rapidity

$$\hat{\alpha} = -\frac{1}{2}\mathrm{artanh}\left[\frac{2T^{tx}}{T^{tt}+T^{xx}}\right] \tag{130}$$

in the x-direction, which corresponds to local velocity $V = -\tanh\hat{\alpha}$ of the plasma. This results in the relations

$$\begin{aligned} T^{tt} &= \varepsilon\cosh^2\hat{\alpha} + p_x\sinh^2\hat{\alpha} & T^{tx} &= -\frac{\varepsilon+p_x}{2}\sinh 2\hat{\alpha} \\ T^{xx} &= \varepsilon\sinh^2\hat{\alpha} + p_x\cosh^2\hat{\alpha} & T^{yy} &= p_y\,. \end{aligned} \tag{131}$$

We can solve the relations (131) for the hydrodynamic quantities and eliminate the rapidity which results in

$$\varepsilon = \frac{1}{2}\left[T^{tt} - T^{xx} + \sqrt{(T^{tt}+T^{xx})^2 - 4(T^{tx})^2}\right] \tag{132}$$

$$p_x = \frac{1}{2}\left[-T^{tt} + T^{xx} + \sqrt{(T^{tt}+T^{xx})^2 - 4(T^{tx})^2}\right] \tag{133}$$

$$p_y = T^{yy}\,. \tag{134}$$

4.5 Viscous hydrodynamics and free streaming

The two most popular models for the dynamics of QGP are free streaming and hydrodynamics. Free streaming models the plasma as a noninteracting dust with the

initial energy density given by the holographic model. The time development is simply described by the free flow and the corresponding energy-momentum tensor. Viscous hydrodynamics gives us the pressure anisotropy as a function of local velocity and energy density. This involves more input data but is ab initio a more natural way of obtaining results.

The hydrodynamic energy momentum tensor consists of the ideal fluid tensor and additional viscous corrections up to desired order. It can thus be expressed as

$$T^{\alpha\beta}_{\text{viscous}} = (\varepsilon + p_{\text{ideal}})\, u^\alpha u^\beta + p_{\text{ideal}}\, \eta^{\alpha\beta} + \Pi^{\alpha\beta}\,. \tag{135}$$

We define the projection operator

$$\Delta^{\mu\nu} = \eta^{\mu\nu} + u^\mu u^\nu \tag{136}$$

and the fluid shear tensor

$$\sigma^{\mu\nu} = 2^{\langle}\partial^\mu u^{\nu\rangle}\,. \tag{137}$$

Here we used the transverse and traceless projection

$$^{\langle}A^{\mu\nu\rangle} \equiv \frac{1}{2}\Delta^{\mu\alpha}\Delta^{\nu\beta}(A_{\alpha\beta} + A_{\beta\alpha}) - \frac{1}{2}\Delta^{\mu\nu}\Delta^{\alpha\beta}A_{\alpha\beta} \equiv A^{\langle\mu\nu\rangle}. \tag{138}$$

With these definitions we can write the first and second order viscous corrections [53] for a conformal fluid as

$$\Pi^{\alpha\beta}_{(1)} \equiv -\eta\sigma^{\alpha\beta} - \zeta\theta\Delta^{\alpha\beta} \tag{139}$$

and

$$\Pi^{\alpha\beta}_{(2)} = \eta\tau_\Pi\left[^{\langle}D\sigma^{\alpha\beta\rangle} + \frac{1}{2}\sigma^{\alpha\beta}\theta\right] + \cdots\,, \tag{140}$$

where the directional derivative is

$$D \equiv u^\alpha\partial_\alpha = -u_t\partial_t + u_x\partial_x \quad \text{and} \quad \theta \equiv \partial_\rho u^\rho. \tag{141}$$

The three dots indicate the curvature and vorticity terms we have omitted. The two parameters η and ζ are the shear and bulk viscosities, respectively. The new parameter τ_Π appearing in the second order is the relaxation timescale of the fluid.

Especially for the directional derivative of the shear tensor we find

$$D\sigma^{\alpha\beta} = 2(D\theta)M^{\alpha\beta} + 2\theta DM^{\alpha\beta}\,, \tag{142}$$

where

$$M^{\alpha\beta} \equiv \frac{\partial^{\langle\alpha}u^{\beta\rangle}}{\theta}\,. \tag{143}$$

The first term in (142) is obviously transverse and traceless and the second term projects to zero.

Using the first order expressions together with relations (133) and (134) results in the rest-frame pressure anisotropy given by

$$p_{x,\text{hydro}} - p_{y,\text{hydro}} = -2\eta\theta. \tag{144}$$

Moving to second order one finds

$$\Pi^{\alpha\beta} \equiv \Pi^{\alpha\beta}_{(1)} + \Pi^{\alpha\beta}_{(2)} = 2\eta \left(-\theta + \tau_\Pi \left(D\theta + \frac{1}{2}\theta^2 \right) \right) M^{\alpha\beta} \tag{145}$$

and

$$p_{x,\text{hydro}} - p_{y,\text{hydro}} = 2\eta \left(-\theta + \tau_\Pi \left(D\theta + \frac{1}{2}\theta^2 \right) \right) . \tag{146}$$

The implementation of this formula is less complicated if one chooses an explicit parameterization for the fluid velocity. Using hyperbolic functions gives the transverse and traceless matrix a rather simple form.

The shear and bulk viscosities of the conformal fluid can be found from [54] and read

$$\eta = \frac{1}{16\pi G_N} \left(\frac{4}{3}\pi T \right)^2 \quad \text{and} \quad \zeta = 0\,. \tag{147}$$

The equilibrium temperature can be solved from the relation

$$\varepsilon = \frac{2}{16\pi G_N} \left(\frac{4}{3}\pi T \right)^3 , \tag{148}$$

which determines the shear viscosity in terms of the known energy density. For numerical results one also needs the value of the relaxation time τ_Π. From [54] we find the value

$$\tau_\Pi = \frac{3}{4\pi T} \left[1 + \frac{1}{3}\text{Harmonic}\left(-\frac{1}{3} \right) \right] \approx \frac{0.180}{T}\,. \tag{149}$$

for a 2+1 dimensional conformal fluid.

We also want to compare our results with the free-streaming model, in which the energy density is modeled with a noninteracting light-like dust. In this scenario, the energy momentum tensor is

$$T^{\mu\nu}(x,t) = \int \frac{d^2k}{k^0}\, k^\mu k^\nu f(x,k,t)\,. \tag{150}$$

We assume the initial distribution to factorize into a product of spatial and momentum parts. The momentum part is further assumed to depend only on the total momentum i.e. energy. This results in the expression

$$f(\mathbf{x},\mathbf{k}) = n(\mathbf{x})F(\mathbf{k}) = n(x)F(k)\,. \tag{151}$$

As we assume the dust to be noninteracting, the time development is simply

$$f(\mathbf{x},\mathbf{k},t) = n(\mathbf{x}-\mathbf{v}t)F(\mathbf{k}) = n(x-v_x t)F(k)\,. \tag{152}$$

Using the parametrization

$$k_x = k\cos\phi, \quad k_y = k\sin\phi, \quad v_x = \cos\phi, \quad v_y = \sin\phi. \tag{153}$$

the energy momentum tensor has the components

$$\begin{aligned}
T_{00}(x,t) &= \int d^2k \frac{(k^0)^2}{k^0} f(\mathbf{x},\mathbf{k},t) = \int_0^{2\pi} d\phi\, n(x-t\cos\phi)\int k^2 dk F(k) \\
T_{xx}(x,t) &= \int d^2k \frac{(k_x)^2}{k^0} f(\mathbf{x},\mathbf{k},t) = \int_0^{2\pi} d\phi\, \cos^2\phi\, n(x-t\cos\phi)\int k^2 dk F(k) \\
T_{yy}(x,t) &= \int d^2k \frac{(k_y)^2}{k^0} f(\mathbf{x},\mathbf{k},t) = \int_0^{2\pi} d\phi\, \sin^2\phi\, n(x-t\cos\phi)\int k^2 dk F(k) \\
T_{xy}(x,t) &= \int d^2k \frac{k_x k_y}{k^0} f(\mathbf{x},\mathbf{k},t) = \int_0^{2\pi} d\phi\, \cos\phi\sin\phi\, n(x-t\cos\phi)\int k^2 dk F(k)\,.
\end{aligned} \tag{154}$$

The momentum integral

$$\varepsilon_0 = 2\pi\int_0^\infty k^2 dk F(k) \tag{155}$$

is not phenomenologically relevant and plays a role of an overall normalization. This means that we do not have to specify the momentum function $F(k)$.

For actual comparisons with hydrodynamics and free streaming, we need to drop some of the generality and fix the source. One natural choice was to assume a Gaussian dependence on both time and the anisotropic spatial coordinate and write

$$\varphi(t,x) = \epsilon\left(1+e^{-\mu^2x^2}\right)e^{-\frac{(t-v)^2}{\sigma^2}}\,. \tag{156}$$

This ansatz was substituted to the previously found expression for the energy-momentum and the corresponding energy density and pressures extracted. Fixing numerical values allows us to plot our results together with the predictions of free streaming and hydrodynamics.

Using the explicit formulas for the energy-momentum and the rest-frame transformations (132)-(134) we get the plots given in figure 12. The dispersion of energy density is quite small during the timescales presented here, even though there is a transverse flow. The phenomenon is more visible in the velocity plot, which lacks a backround value. It is good to note that the dynamics is not driven by the gaussian time dependence of the source (156), which happens at very small timescales compared to the ones used in the plots.

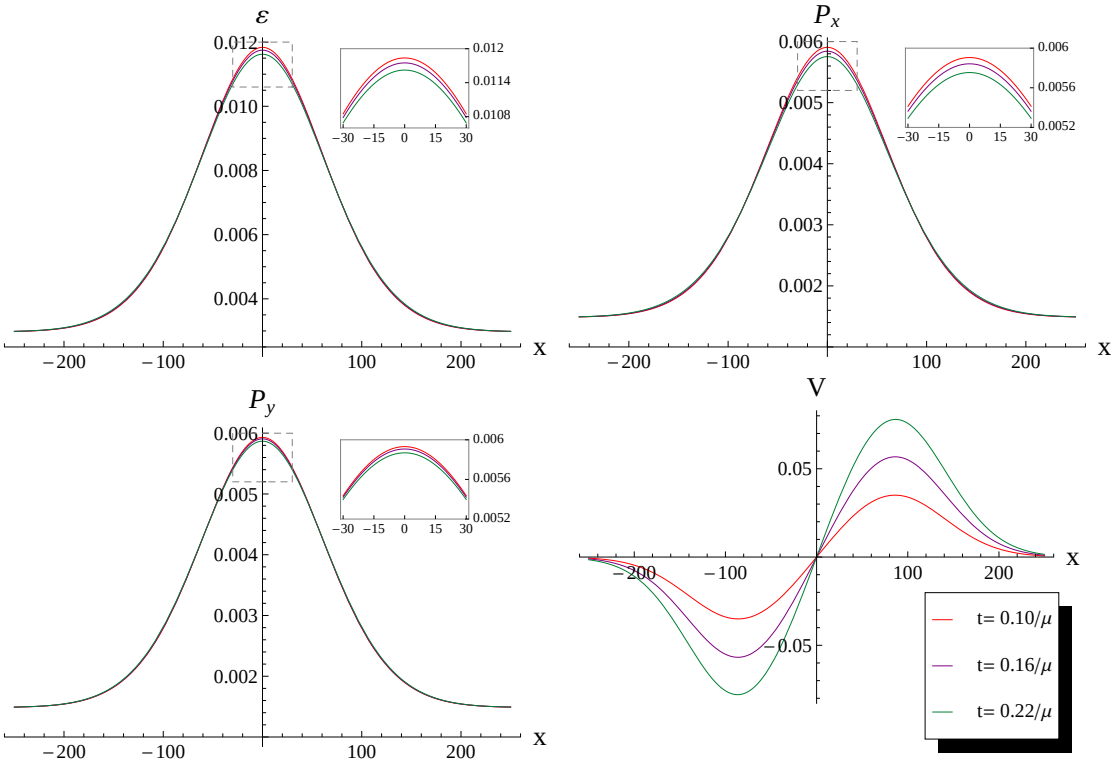

Figure 12: The energy density in the rest frame $\varepsilon = p_x + p_y$, pressures p_x and p_y with parameter values $\nu = 0.5$, $\sigma^2 = 0.1$, $\mu = 0.01$ and $\epsilon = 0.005$.

The local energy density and velocity data obtained is used as an input in viscous hydrodynamics, whereas the initial energy density and velocity determine the form of the energy distribution in the free streaming model.

Our main motivation to generalize the scalar collapse to the case with anisotropic initial conditions was to examine pressure anisotropies in the boundary theory. The predictions and time development of the anisotropy in different models is compared in figure 13. The difference in longitudinal and transverse pressure is not very large compared to the overall values, as we can see from the vertical scale.

The plot shows good agreement with the established models. In early times, the two nonholographic predictions disagree. It is good to note that holography follows the free streaming result, which is probably most justified in the initial stages. The rapid agreement of the two models is in fact more puzzling than the early disagreement, but holography seems to perform reasonably in both regimes.

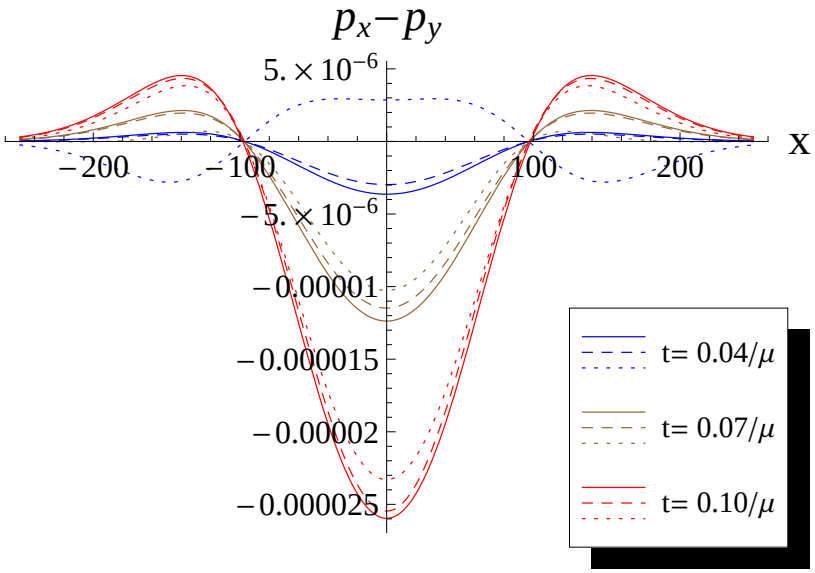

Figure 13: The holographic prediction for pressure anisotropy (solid lines) compared with those resulting from second order hydrodynamics (dotted) and free streaming (dashed).

Various other configurations can be examined in a similar way. The combination of two Gaussian peaks

$$\varphi(t,x) = \epsilon \left(1 + e^{-\mu^2\left(x-\frac{d}{2}\right)^2} + e^{-\mu^2\left(x+\frac{d}{2}\right)^2}\right) e^{-\frac{(t-\nu)^2}{\sigma^2}} \tag{157}$$

with two different separation distances d gives quite natural-looking plots of energy density and pressure anisotropy. Figure 14 shows the form of energy density and pressure anisotropy in two cases with overlapping and more separated Gaussian sources.

As before, holography initially follows the more natural free-steaming solution and agrees with both classical models at later times.

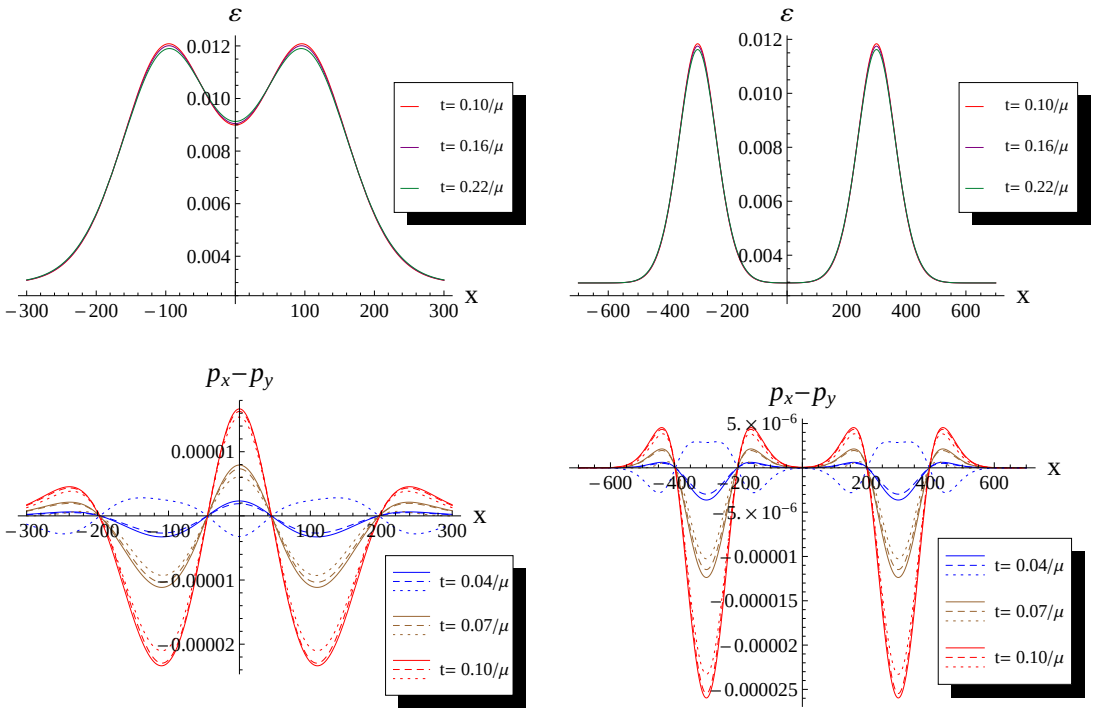

Figure 14: The energy density ε in the rest frame and the spatial profile of the pressure anisotropy obtained in the AdS/CFT computation (solid lines) compared with those from second order hydrodynamics (dotted) and free streaming (dashed). The source profile has the form (157), with $\nu = 0.5$, $\sigma^2 = 0.1$, $\mu = 0.01$ and $\epsilon = 0.005$. The left column corresponds to $d = 2/\mu$, the right one to $d = 6/\mu$.

5 Conclusions and outlook

The QGP-results obtained from holography look promising even though we have been forced to restrict ourselves to a rather small interval in space and time to keep within the domain of validity of naive perturbation theory. One could also proceed to more realistic and adjustable initial parameters by using a large number of Gaussians to build up the desired injection of energy. Increasing the validity domain is a very interesting direction but seems to require resummed perturbation theory. Despite these limitations, our work is a major generalization of the preceding isotropic models and enables more realistic holographic modeling of strongly coupled plasmas.

Our investigation into hyperscaling violating Lifshitz-Vaidya has somewhat less direct physical applications. Nevertheless, it acts as a first study of this sort and provides a numerical verification of the linearizing time dependence of entanglement entropy. Moreover, it verifies the predictions made on the speed of thermalization in these models.

References

[1] J. Maldacena, "The Large N Limit of Superconformal Field Theories and Supergravity," Adv.Theor.Math.Phys. **2:**231-252 (1998) [hep-th/9711200]

[2] L. Susskind, "The world as a hologram", J. Math. Phys **36**, (1995)

[3] S. Gubser, I. R. Klebanov, and A. M. Polyakov, Gauge theory correlators from noncritical string theory, Phys.Lett. **B428** (1998) 105–114, arXiv: hep-th/9802109

[4] E. Witten, Anti-de Sitter space and holography, Adv.Theor.Math.Phys. **2** (1998) 253–291, arXiv:hep-th/9802150

[5] Geoffrey Compère, Paul McFadden, Kostas Skenderis, Marika Taylor: The holographic fluid dual to vacuum Einstein gravity JHEP 07(2011)050, arXiv:1103.3022

[6] I. Bredberg, C. Keeler, V. Lysov and A. Strominger, From Navier-Stokes To Einstein, [arXiv:1101.2451].

[7] J. Brown, J. York, "Quasilocal energy and conserved charges derived from the gravitational action", Phys. Rev. **D47** (1993)

[8] S. S. Gubser, A. Nellore, "Ground states of holographic superconductors," Phys. Rev. **D80** (2009) 105007. [arXiv:0908.1972 [hep-th]].

[9] S. A. Hartnoll, J. Polchinski, E. Silverstein, D. Tong, "Towards strange metallic holography," JHEP **1004**, 120 (2010). [arXiv:0912.1061 [hep-th]].

[10] S. A. Hartnoll, A. Tavanfar, "Electron stars for holographic metallic criticality," Phys. Rev. **D83** (2011) 046003. [arXiv:1008.2828 [hep-th]].

[11] C. Charmousis, B. Gouteraux, B. S. Kim, E. Kiritsis and R. Meyer, "Effective Holographic Theories for low-temperature condensed matter systems," JHEP **1011**, 151 (2010) [arXiv:1005.4690 [hep-th]].

[12] S. A. Hartnoll, "Horizons, holography and condensed matter," [arXiv:1106.4324 [hep-th]]

[13] S. Sachdev, "Condensed Matter and AdS/CFT," [arXiv:1002.2947 [hep-th]].

[14] S. N. Solodukhin, "Entanglement Entropy in Non-Relativistic Field Theories," JHEP **1004**, 101 (2010) [arXiv:0909.0277 [hep-th]].

[15] M. Alishahiha, M. R. Mohammadi Mozaffar and A. Mollabashi, "Fermions on Lifshitz Background," Phys. Rev. D **86** (2012) 026002 [arXiv:1201.1764 [hep-th]].

[16] M. Wolf, "Violation of the entropic area law for Fermions," Phys. Rev. Lett. **96**, (2006) [arXiv:0503219 [quant-ph]]

[17] X. Dong, S. Harrison, S. Kachru, G. Torroba and H. Wang, "Aspects of holography for theories with hyperscaling violation," JHEP **1206** (2012) 041 [arXiv:1201.1905 [hep-th]].

[18] E. Shaghoulian, Holographic entanglement entropy and Fermi surfaces, JHEP **05** (2012) 065 [arXiv:1112.2702]

[19] P. Vaidya, "The Gravitational Field of a Radiating Star," Proc. Indian Acad. Sci. **A33** (1951) 264.

[20] W. B. Bonnor, P. C. Vaidya, "Spherically symmetric radiation of charge in Einstein-Maxwell theory," Gen. Rel. Grav. **1** (1970) 127-130.

[21] V. Balasubramanian, A. Bernamonti, J. de Boer, N. Copland, B. Craps, E. Keski-Vakkuri, B. Muller, A. Schafer *et al.*, "Thermalization of Strongly Coupled Field Theories," Phys. Rev. Lett. **106** (2011) 191601. [arXiv:1012.4753 [hep-th]].

[22] V. Balasubramanian, A. Bernamonti, J. de Boer, N. Copland, B. Craps, E. Keski-Vakkuri, B. Muller, A. Schafer *et al.*, "Holographic Thermalization," Phys. Rev. **D84** (2011) 026010. [arXiv:1103.2683 [hep-th]].

[23] K. Goldstein, S. Kachru, S. Prakash and S. P. Trivedi, "Holography of Charged Dilaton Black Holes," JHEP **1008**, 078 (2010) [arXiv:0911.3586 [hep-th]].

[24] V. Keränen, E. Keski-Vakkuri and L. Thorlacius, "Thermalization and entanglement following a non-relativistic holographic quench," Phys. Rev. D **85** (2012) 026005 [arXiv:1110.5035 [hep-th]].

[25] J. Tarrio, S. Vandoren, "Black holes and black branes in Lifshitz spacetimes," JHEP **1109**, 017 (2011). [arXiv:1105.6335 [hep-th]].

[26] L. Huijse, S. Sachdev and B. Swingle, "Hidden Fermi surfaces in compressible states of gauge-gravity duality," Phys. Rev. B **85**, 035121 (2012) [arXiv:1112.0573 [cond-mat.str-el]].

[27] M.Alishahiha,E. O'Colgain, H. Yavartanoo: Charged Black Branes with Hyperscaling Violating Factor, JHEP11(2012)137

[28] S. Kachru, X. Liu and M. Mulligan, "Gravity Duals of Lifshitz-like Fixed Points," Phys. Rev. D **78** (2008) 106005 [arXiv:0808.1725 [hep-th]].

[29] M. Alishahiha, A. F. Astaneh and M. R. M. Mozaffar, "Thermalization in Backgrounds with Hyperscaling Violating Factor," arXiv:1401.2807 [hep-th].

[30] J. B. Hartle and S. W. Hawking, "Path Integral Derivation of Black Hole Radiance," Phys. Rev. D **13** (1976) 2188.

[31] V. Hubeny, H. Maxfield, "Holographic probes of collapsing black holes" JHEP **1203** (2014) 097 [arXiv:1312.6887 [hep-th]]

[32] S. Ryu, T. Takayanagi, "Holographic derivation of entanglement entropy from AdS/CFT," Phys. Rev. Lett. **96** (2006) 181602. [hep-th/0603001].

[33] S. Ryu, T. Takayanagi, "Aspects of Holographic Entanglement Entropy," JHEP **0608** (2006) 045. [hep-th/0605073].

[34] V. E. Hubeny, M. Rangamani and T. Takayanagi, "A Covariant holographic entanglement entropy proposal," JHEP **0707** (2007) 062 [arXiv:0705.0016 [hep-th]].

[35] R. Callan, J. -Y. He and M. Headrick, "Strong subadditivity and the covariant holographic entanglement entropy formula," JHEP **1206** (2012) 081 [arXiv:1204.2309 [hep-th]].

[36] H. Liu and S. J. Suh, "Entanglement Tsunami: Universal Scaling in Holographic Thermalization," arXiv:1305.7244 [hep-th].

[37] H. Liu and S. J. Suh, "Entanglement growth during thermalization in holographic systems," arXiv:1311.1200 [hep-th].

[38] H. Kouno, M. Maruyama, F. Takagi, and K. Saito, "Relativistic hydrodynamics of quark-gluon plasma and stability of scaling solutions," Phys. Rev. D **41**, 2903 (1990)

[39] D. Teaney, "Viscous Hydrodynamics and the Quark Gluon Plasma," [arXiv:0905.2433 [nucl-th]]

[40] P. Kovtun, D. T. Son and A. O. Starinets, "Viscosity in strongly interacting quantum field theories from black hole physics," Phys. Rev. Lett. **94**, 111601 (2005) [hep-th/0405231].

[41] A. Buchel and J. T. Liu, "Universality of the shear viscosity in supergravity," Phys. Rev. Lett. **93**, 090602 (2004) [hep-th/0311175].

[42] G. Policastro, D. T. Son and A. O. Starinets, "The Shear viscosity of strongly coupled N=4 supersymmetric Yang-Mills plasma," Phys. Rev. Lett. **87**, 081601 (2001) [hep-th/0104066].

[43] S. Bhattacharyya and S. Minwalla, JHEP **0909** (2009) 034 [arXiv:0904.0464 [hep-th]].

[44] G. Beuf, M. P. Heller, R. A. Janik and R. Peschanski, "Boost-invariant early time dynamics from AdS/CFT," JHEP **0910** (2009) 043 [arXiv:0906.4423 [hep-th]].

[45] J. L. Albacete, Y. V. Kovchegov and A. Taliotis, "Modeling Heavy Ion Collisions in AdS/CFT," JHEP **0807** (2008) 100 [arXiv:0805.2927 [hep-th]].

[46] J. L. Albacete, Y. V. Kovchegov and A. Taliotis, "Asymmetric Collision of Two Shock Waves in AdS(5)," JHEP **0905** (2009) 060 [arXiv:0902.3046 [hep-th]].

[47] P. M. Chesler and L. G. Yaffe, "Holography and colliding gravitational shock waves in asymptotically AdS_5 spacetime," Phys. Rev. Lett. **106** (2011) 021601 [arXiv:1011.3562 [hep-th]].

[48] M. P. Heller, R. A. Janik and P. Witaszczyk, "The characteristics of thermalization of boost-invariant plasma from holography," Phys. Rev. Lett. **108** (2012) 201602 [arXiv:1103.3452 [hep-th]].

[49] M. P. Heller, R. A. Janik and P. Witaszczyk, "A numerical relativity approach to the initial value problem in asymptotically Anti-de Sitter spacetime for plasma thermalization - an ADM formulation," Phys. Rev. D **85**, (2012)

[50] P. M. Chesler and L. G. Yaffe, "Horizon formation and far-from-equilibrium isotropization in supersymmetric Yang-Mills plasma," Phys. Rev. Lett. **102** (2009) 211601 [arXiv:0812.2053 [hep-th]].

[51] R. A. Janik, R. B. Peschanski, "Asymptotic perfect fluid dynamics as a consequence of Ads/CFT," Phys. Rev. **D73**, 045013 (2006). [hep-th/0512162]

[52] S. de Haro, S. N. Solodukhin and K. Skenderis, "Holographic reconstruction of space-time and renormalization in the AdS / CFT correspondence," Commun. Math. Phys. **217** (2001) 595 [hep-th/0002230].

[53] R. Baier, P. Romatschke, D. T. Son, A. O. Starinets and M. A. Stephanov, "Relativistic viscous hydrodynamics, conformal invariance, and holography," JHEP **0804** (2008) 100 [arXiv:0712.2451 [hep-th]].

[54] S. Bhattacharyya, R. Loganayagam, I. Mandal, S. Minwalla and A. Sharma, "Conformal Nonlinear Fluid Dynamics from Gravity in Arbitrary Dimensions," JHEP **0812** (2008) 116 [arXiv:0809.4272 [hep-th]].